AN INVESTIGATION OF ELECTRIC FIELD INDUCED SURFACE DIFFUSION AND MICRO/NANO-SCALE ISLAND GROWTH: EXPERIMENTS AND MODELING.

BY:

VINAYPREET S. GILL

SC.M., BROWN UNIVERSITY, 2006

M.S., UNIVERSITY OF DAYTON, 2003

BACHELOR OF ENGINEERING, THAPAR UNIVERSITY, 2001

A DISSERTATION SUBMITTED IN PARTIAL FULFILLMENT OF THE REQUIREMENTS FOR THE DEGREE OF DOCTOR OF PHILOSOPHY IN THE DIVISION OF ENGINEERING AT BROWN UNIVERSITY

PROVIDENCE, RHODE ISLAND

MAY 2009

This Dissertation by Vinaypreet S. Gill is accepted in its present form by the Division of Engineering as satisfying the dissertation requirement for the degree of Doctor of Philosophy.

Date _____ _____

Professor Pradeep Guduru, Advisor

Recommended to the Graduate Council

Date _____ _____

Professor Allan Bower, Reader

Date _____ _____

Professor Brian Sheldon, Reader

Approved by the Graduate Council

Date _____ _____

Professor Sheila Bonde

Dean of the Graduate School

Curriculum Vitae

Education

- **Brown University**, Providence, RI.

  Ph. D. Engineering (Solid Mechanics) July 2008

  (Minor: Materials Science)

  Dissertation: An Investigation of Electric Field Induced Surface Diffusion and Micro/Nano Scale Island Growth: Experiments and Modeling

  Sc. M. Applied Mathematics May 2006

- **University of Dayton**, Dayton, Ohio.

  M.S. Mechanical Engineering May 2003

  Dissertation: Nano-characterization of Bio-Silica using Ultrasonic and Atomic force microscopy

- **Thapar University**, Patiala, India.

  Bachelor of Engineering, **Mechanical Engineering** May 2001

Publications

1. **V.Gill,** P.R.Guduru, B.W.Sheldon, Electric field induced surface diffusion and micro/nano-scale island growth, *International Journal of Solids and Structures 45(2008), pp. 943-958*.
2. **Vinaypreet S.Gill,** Kevin P.Hallinan, N.S.Brar, Nanocharacterization of bio-silica using Atomic force and Ultrasonic force Microscopy, *Proceedings of SPIE-Volume 5852(2004), pp.751-757*.

Honors and Awards

- University fellowship from Graduate School at Brown University. 2003

Acknowledgements

At the end of this effort, I feel great pleasure in thanking some of the people who made this work possible and the last five years some of the most memorable of my life.

First of all I would like to thank my Graduate Advisor, Prof. Pradeep Guduru, for guiding me through this project. He was always patient, thoughtful and full of ideas to get me through some tough roadblocks.

I would also like to thank Prof. Allan Bower and Prof. Brian Sheldon for helping me through some very important phases of the work. This project would not have come to fruition without their guidance.

I am extremely thankful to the entire faculty in the Division of Engineering for being so helpful and approachable. The same goes for our administrative staff, especially Stephanie, Pat and Peggy.

This project will still be incomplete if it were not for the technical staff, especially Michael Jibitsky, Brian Corkum, Charlie Vickers and Mike Packer. They were always most helpful.

I made some lifelong friends in these past five years and they made my stay here fun and memorable. I am thankful to all of them for being there for me in good times and bad. A special thanks to Julie for keeping the lab in working condition.

Last but not the least I would like to thank my family, especially my Uncle Brar for guiding me and being there for me all the time. I will not be here without my family's support.

Brown and the time I spent here will always have a special place in my heart.

Contents

List of Tables

List of Figures

Chapter 1

Introduction and Overview

Fabricating ordered patterns of controlled shape, size and spacing at nanometer and micron scales has been an important goal of nano-scale science and engineering in the recent past. Some of the applications envisaged for such processes include quantum dot devices, nano-composites and high density data storage devices. Most of the existing nanofabrication techniques can be loosely described as either *top-down* type or *bottom-up* type. The *top-down* approach consists of examples such as photolithography, X-ray lithography, electro-deposition, scanning probe or electron beam lithography etc, which typically involve controlled micro and nanoscale material removal (micro and nanoscale surface and bulk machining) to achieve patterned structures. On the other hand, in the *bottom-up* approach, one tries to exploit certain energetic or configurational forces acting at nano- and micro-scales to drive a self-assembly process. Typically, configurational forces arise as a result of a system's attempt to minimize its total free energy and the associated competition between the dominant contributions to the free energy. Some of the most elegant examples of this self-assembly process can be found in nature. The building blocks of living organisms and the molecular structures in them are the most familiar examples of nanoscale self-assembly processes. One example of self-assembly in nature is diatoms, which form exquisite features as seen in Fig. 1.1(a) (Böke et al. 2008). At a slightly larger scale of a few tens to hundreds of nanometers, a well known example

is the strain induced island formation in epitaxial semiconductor thin films. An example of a quantum dot grown on an epitaxial thin film (Medeiros-Rebeiro et al. 1998, Horn et al. 1994) can be seen in Fig. 1.1(b). It shows an STM image of a germanium quantum dot grown on a Silicon (001) surface. Self-assembly processes have a natural appeal for nano-fabrication because, in principle, it is possible to drive a system to the desired final state by simply fine-tuning the initial state and process parameters such as temperature.

However, there are some difficulties in making use of self-assembly processes to fabricate devices of practical use. For example, in the strain driven growth of semiconductor quantum dots, the resulting nanostructures usually do not possess any spatial order and also end up with a non-uniform size distribution because the island locations are determined by random initiation sites. Thus, it is desirable to have a technique that can combine the driving configurational forces that underlie self-assembly processes and the spatial control that can be achieved in top-down processes. One of the goals of this work is to suggest that spatial and size control can be achieved through a guiding electric field on the surface of electrically conductive materials. It is shown that, at sufficiently high temperatures, a gradient in electric field on the surface of a conductor can induce diffusion, leading to surface evolution (Gill et al. 2008).

Surface diffusion is a common phenomenon in metals and semiconductors when the temperature is high enough to promote mobility of surface atoms. In the presence of one or more energetic driving forces, mobile atoms migrate on external surfaces or internal surfaces such as grain boundaries, leading to evolution of the topography of these surfaces. In many situations of engineering interest, the energetic driving force is often provided by an attempt to minimize the elastic energy (i.e. an attempt to relieve stresses)

or the total surface energy (i.e. an attempt to minimize surface curvature variations). It is well recognized that surface diffusion plays a central role in a wide range of phenomena such as deformation and fracture of materials, fabrication processes such as powder metallurgy and sintering, spheroidization of inclusions in alloys, etc. For example, in polycrystalline materials, surface diffusion due to stress gradients leads to deformation modes such as creep (Rubinstein, 1983); the singular stress field at the tip of a crack in an elastic material provides energetic driving force for surface diffusion along the crack faces, leading *creep crack propagation* (Chuang and Rice, 1973). Surface diffusion becomes very important in nano- and micro-scale structures where the characteristic length of diffusion becomes comparable to the dimensions of the structure. In such cases, surface evolution mediated by diffusion leads to significant changes in size, shape and morphology.

Surface diffusion can be exploited to derive practical nano-scale self-assembly technologies such as *strain induced island growth* in semiconductors to fabricate useful structures such as quantum dots. A self assembly process is typically the result of competition between the dominant contributions to the free energy while attempting to minimize the total free energy. For example, in case of *strain induced island growth* in semiconductor thin films, small surface perturbations simultaneously lead to an increase in the surface energy and a decrease in the elastic energy of the film. The competition between these two energy changes drives a self-assembly process by which an initially uniform film can evolve into isolated islands (eg. quantum dots).

In the context of achieving spatial and size control on a nano-scale assembly process driven by an energetic driving force, some relevant question are: what other

energetic driving forces can act at a solid surface at the relevant length scale, besides that due to strain energy, which can drive surface evolution? Can they be exploited to gain control on nano and micro-scale patterning?

One of the objectives of this work is to demonstrate that surface diffusion and evolution in electrically conducting materials such as metals and semiconductors can be driven by electric fields. It is, in principle, possible to control spatial and size distribution of nano and micro-scale surface patterning through an appropriate guiding *electric field* and the energetic driving force that it generates on the surface of electrically conductive materials.

Influence of electric fields on surface evolution through diffusion has other important practical consequences as well. Reliability of micro-contact switches in NEMS and MEMS devices, which are often made of gold, is influenced by surface roughness of contact interfaces (Du and Srolovitz, 2004). The contacting surfaces are repeatedly subjected to very strong electric field each time they are brought into contact during on-off cycles. Since contact is localized at a few peaks of the rough interface, they are subjected local Joule heating, in addition to mechanical loading. The elevated temperature increases the mobility of surface atoms, which can lead to surface evolution provided there is a driving force due to the strong electric field. Thus, it is very important to understand how surface roughness evolves under strong electric fields in order to quantify and predict life time and reliability of contact switches.

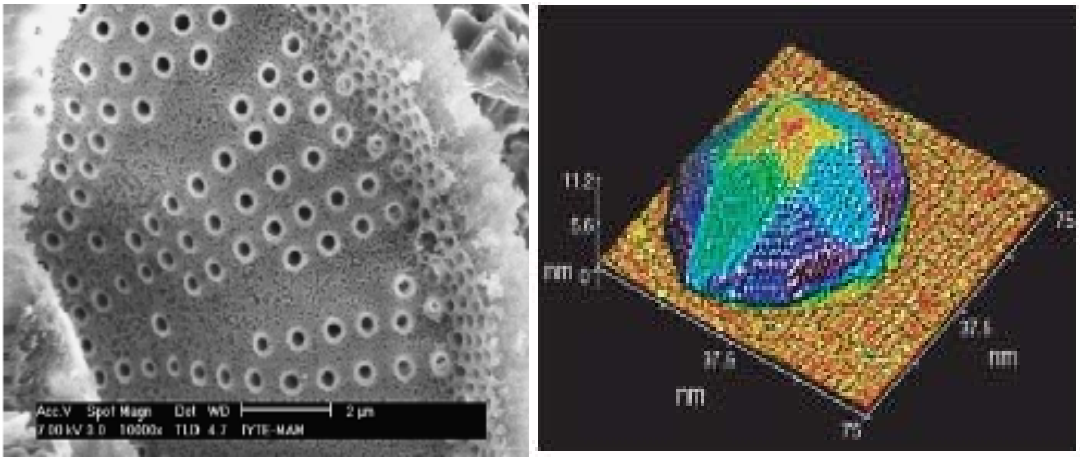

(a) *(b)*

Figure 1.1: Examples of self-assembly (a) An electron micrograph of a naturally growing diatom [Böke et al. 2008]. (b) A Ge quantum dot growing on Si (001) surface [Medeiros-Rebeiro et al. 1998]. (Reproduced with permission from the publisher).

The basic idea that surface atoms can be manipulated and forced to move by means of strong electric fields present at Scanning Tunneling Microscope (STM) tips is known for over a decade. There have been articles reporting evolution of surface morphology under STM scanning (Avouris, 1995; Li et al. 1996; Dulot et al. 2000; Murphy et al. 2003). Avouris [1995] discusses several types of interactions between an STM tip and individual surface atoms by which the latter can be manipulated. Li et al. [1996] demonstrated the influence of STM tip on the atomic motion of Ag on Ag (110) and showed that the tip can displace monoatomic steps over distances as large as several tens of nanometers. Dulot et al. [2000] showed that the surface morphology of copper changes drastically upon repeated STM scanning even under standard tunneling parameters. Similar results were reported by Murphy et al. [2003] on Fe surfaces as illustrated in Fig 1.2(a) and 1.2(b), which show considerable roughening of the Fe films after several minutes of scanning with a STM tip. Although such observations were

accompanied by qualitative descriptions of possible surface diffusion aided by the strong electric field present between the STM tip and the sample surface, there were no attempts to develop a quantitative description of the phenomenon. Later, at the same time the work presented in this thesis was being carried out, Du and Srolovitz [2004] independently presented a study of the stability of a surface in a parallel plate capacitor in the context of how electric fields can have undesirable surface roughening effect in nano and micro-scale contact switches in NEMS and MEMS devices. They showed that there exists a critical wavelength, above which perturbations are energetically admissible and calculated the fastest growing perturbation wavelength. Their analysis suggested that for two initially parallel gold surfaces separated by 10nm with and applied voltage of 10 V, the wavelength of the fastest growing perturbation would be approximately 200 nm and a corresponding growth time constant of $\sim 50s$ at room temperature. These estimates demonstrate that surface diffusion under the influence of electric fields needs to be considered in designing in several practical devices. More recently, Yang and Song [2005] presented a similar analysis, considering the effect of elastic energy as well. Chiu et al. [2006a, b] numerically studied the problem of surface instability under a uniform electric field and confirmed the predictions of the Du and Srolovitz [2004] analytical model. However, experimental studies of electric field induced surface diffusion have been limited to the context of STM tip – surface interaction and its undesirable effects on STM imaging. Besides individual atom manipulation (Avouris, 1995), its potential to fabricate surface structures at nano to micrometer scales remains untapped. The work presented in this thesis is intended to be a starting point in developing a potential micro/nano-scale surface fabrication technique based on electric field induced surface

diffusion. The main objectives of the work described here are to (i) experimentally study of the phenomenon of electric field induced surface diffusion in conductive materials; (ii) simulate the kinetics of surface evolution under the influence of an external electric field; (iii) develop sufficient understanding of experimental parameters so that isolated islands can be grown in any desired spatial pattern and size distribution.

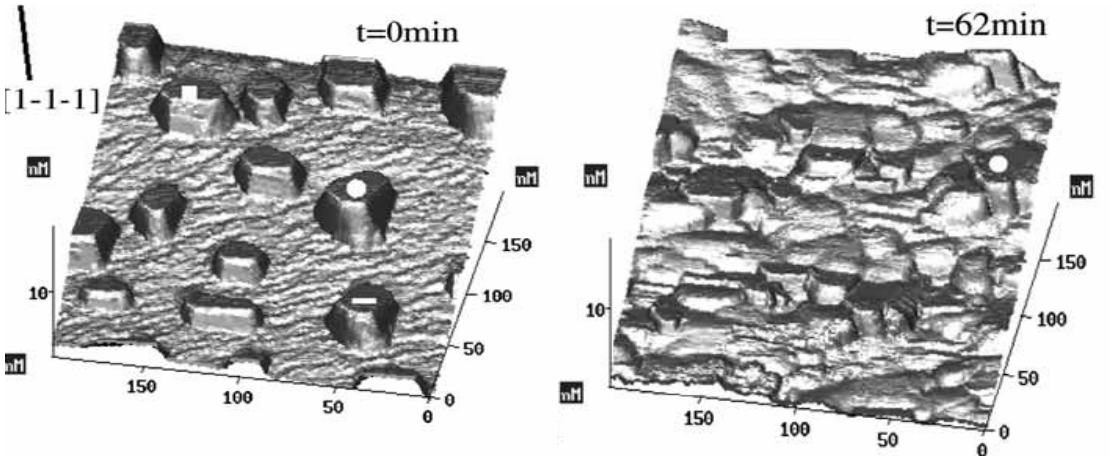

(a) *(b)*

Figure 1.2: STM images taken with a MnNi tip of the same 200nm x 200nm are of a 6 Angstrom Fe film grown on vicinal Mo(100) surface at 760±15 K shows considerable surface diffusion driven by the electrostatic field between the tip and the Fe surface over 62 minutes.[Murphy et.al. 2003] (Reprinted with permission from the publisher)

It is important to note the distinction between the phenomenon under discussion here and the recent work in literature on processes such as Lithographically Induced Surface Assembly (LISA) or Lithographically Induced Surface Construction (LISC) and other similar techniques (Chou and Zhuang, 1999a, b; Suo and Liang, 2001, Leach et al. 2005; Xiang et al, 2004; Schaeffer, 2000; Kim and Lu, 2006a, b; Lu and Kim, 2006). The main idea in such techniques is (Fig. 1.3), if a polymer film above its glass transition temperature is subjected to an electric field using a patterned electrode, the film flows by

electrostatic attraction and tends to take the shape of the electrode. Alternatively, the liquid like polymer film can also become unstable under a uniform field and evolves into islands. It is important to note that such techniques deal with dielectric polymers or liquids in which the mechanism of shape change is bulk flow of the polymer (governed by the Navier-Stokes equation); whereas the phenomenon under discussion in this thesis pertains to conducting materials such as metals and doped semiconductors and the mechanism of shape evolution is surface diffusion.

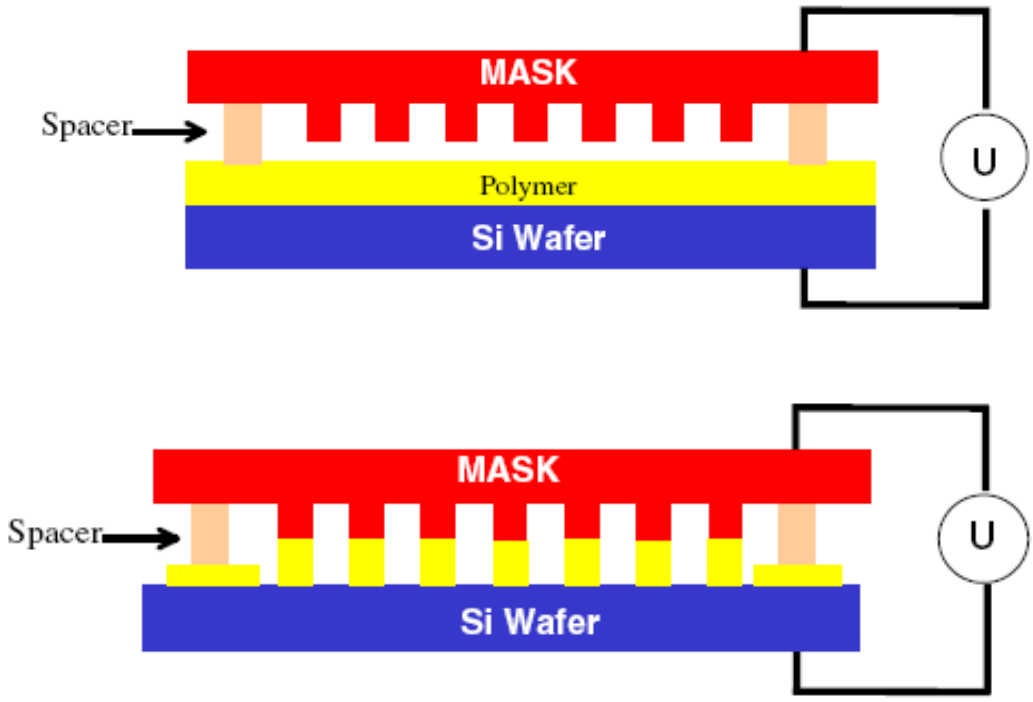

Figure 1.3: Lithographically induced surface construction (LISC) in polymers showing bulk flow of polymer subjected to electric field using a patterned electrode [Lie et al. 2003]. (Reprinted with permission from the publisher).

This thesis presents a study of surface diffusion induced by the application of an electric field to form nano/micro scale islands and it is organized as follows. The driving

force on a surface due to a focused electric field is demonstrated first through an energetic argument, followed by an examination of the stability of a surface in a parallel plate capacitor. Surface evolution in the fringe field of a finite parallel plate capacitor is then analyzed. Results from an experimental investigation on gold surfaces at elevated temperatures are presented next, which demonstrate the growth of micro and nano-scale islands under the influence of applied electric field. The experimental observations raise several issues for future study. Also a numerical study using the finite element analysis (FEA) is carried out and presented to model the kinetics of the phenomenon. The results from these numerical simulations satisfactorily explain the experimental results. Finally, based on the results of this initial study, several suggestions further experimental investigations are proposed.

Chapter 2

An Analysis of Electric Field Induced Surface Diffusion

2.1 Introduction

Various experimental observations, as discussed in chapter 1, suggest that atoms can diffuse and migrate on metallic surfaces under the influence of external electrostatic fields, such as those at an STM tip. Although it has not been investigated experimentally, electrostatic fields in NEMS and MEMS contact switches are conjectured to roughen the contact interfaces, affecting device reliability [Du and Srolovitz, 2004]. Also, Chien et al. [1996] discussed surface roughening of a piezoelectric surface subjected to mechanical and electrical loading and showed that electric loading in certain directions can promote surface roughening through surface diffusion. Thus, it is important to understand the mechanics of electric field induced surface evolution with respect to device reliability.

However, it is possible to exploit the phenomenon for practical benefits as well. If a localized electric field can lead to a localized surface perturbation, then it should be possible to modify surface topography at any desired location and create nano/micro scale surface features. Moreover, in principle, the micro/nano islands can be created in any desired spatial pattern and size distribution by employing an appropriate array of patterned electrodes which applies the localized guiding electric field. Such an array would be akin to a photomask for photolithography; however, instead of being a *top-*

down technique, i.e. etching material away, this method uses the electric field induced configurational force to result in a "guided assembly" of a surface into desired shapes. The main objective of this work is to examine the driving force on a conducting surface due to the presence of electric fields, experimentally demonstrate the phenomenon and numerically simulate the kinetics to understand surface evolution.

2.2 Driving force on a conducting surface due to an electric field

The energetic driving force on a conducting surface due to an external electrical field is considered in this section.

2.2.1 An energetic analysis for a localized electric field

In order to illustrate the driving force on the surface of a conductor due to an electric field, consider the 2-D situation shown in Fig. 2.1(a). An electrode of width w is placed normal to a conducting surface at a distance d and an electric potential difference V is applied between them. The electrode and the surface form a capacitor and an electrostatic field $E = V/d$ is established between them. To simplify the argument, the fringe field near the edges is ignored. In order to determine lower energy configurations of the surface, consider a small sinusoidal, island-like perturbation to the surface under the electrode, as shown in Fig. 2.1(b). Note that such a perturbation does not conserve mass. As a result, the energy change calculations below are only approximate. However, neglecting the fringe field is a bigger approximation. Moreover, a mass conserving perturbation is a matter of choosing a shape whose area with respect to the x-axis is zero; such shapes would complicate the calculation, but do not change the conclusions

qualitatively. Thus, although the following analysis is approximate in a number of ways, it estimates the order of magnitude of the expected island height and motivates the subsequent experimental effort. The perturbation shown in Fig. 2.1(b) increases the surface area and hence the surface energy of the system. The perturbation changes the shape of the gap as well, resulting in a change in the electric potential energy. If the surface is stressed, the perturbation changes the elastic energy as well (Freund, 1995; Srolovitz, 1989). However, in the current context, the solid is assumed to be stress free. The increase in the surface energy can be calculated as

$$\Delta U_s = \gamma \int_{-w/2}^{w/2} \left[\sqrt{1 + (dy/dx)^2} - 1 \right] dx \tag{2.1}$$

Where γ is the surface energy per unit area and y is the shape of the perturbation, given by

$$y(x) = h \cos\left(\frac{\pi x}{w} \right) \tag{2.2}$$

where h is the perturbation amplitude. For small values of the surface slope, Eq. 2.1 can be evaluated as

$$\Delta U_s = \frac{\pi^2 \gamma h^2}{4w} \tag{2.3}$$

The increase in the electrostatic energy in the capacitor is given by

$$\Delta U'_E = \frac{1}{2} V^2 (C_2 - C_1) \tag{2.4}$$

where C_2 and C_1 are capacitances in the presence of and in the absence of the perturbation respectively. C_1 is given by

$$C_1 = \frac{\varepsilon_o w}{d} \tag{2.5}$$

and C_2 can be approximately evaluated as

$$C_2 = \varepsilon_o \int_{-w/2}^{w/2} \frac{dx}{d - y(x)} \tag{2.6}$$

where ε_o is the free space permittivity. Thus, for small values of the perturbation amplitude ($h/d << 1$), the increase in the electrostatic energy can be evaluated as

$$\Delta U'_E = \frac{\varepsilon_o w V^2 h}{\pi d^2} \tag{2.7}$$

Initial charge, Q_1, on the capacitor is C_1V and the final charge, Q_2, is C_2V. The change in the stored charge on the capacitor plates is equal to

$$Q_2 - Q_1 = (C_2 - C_1)V \tag{2.8}$$

and the incremental work done by the external power supply in changing the stored charge is given by

$$\Delta W = -(C_2 - C_1)V^2 \tag{2.9}$$

Thus, the net change in the electrostatic potential energy can be expressed as

$$\Delta U_E = \Delta W + \Delta U'_E = -\frac{\varepsilon_o w V^2 h}{\pi d^2} \tag{2.10}$$

Thus net change in the potential energy of the system due to the perturbation is given by

$$\Delta U = \Delta U_s + \Delta U'_E = \frac{\pi^2 \gamma}{4w} h^2 - \frac{\varepsilon_o w V^2}{\pi d^2} h \tag{2.11}$$

As evident from Eq.2.11, the surface energy and electric energy are in competition with each other. The surface energy tends to stabilize the surface and tries to return it to the

initial flat configuration. On the other hand, the electric energy tends to destabilize the perturbation and helps it grow. This competition determines the equilibrium shape of the perturbation. The change in the potential energy ΔU is schematically plotted as a function of the perturbation amplitude h in Fig. 2.2. Note that ΔU is minimum at h_o given by Eq. 2.13, which corresponds to equilibrium perturbation height h_o, which can be easily calculated by evaluating

$$\frac{d\left(\Delta U\right)}{dh} = 0 \quad . \tag{2.12}$$

which yields

$$h_o = \frac{2\varepsilon_o w^2 E^2}{\pi^3 \gamma} \tag{2.13}$$

where $E = V/d$. Thus, starting from a flat configuration, there is an energetic driving force or a configurational force on the surface to form an island of height h_o. The surface will assume the lower energy shape if there is a physical mechanism to do so. At a sufficiently high temperature, such a mechanism is provided by surface diffusion, which can drive the surface towards the new equilibrium shape. For an electric field of $E = 10^9$ *V/m* and $\gamma \sim 1$ J/m^2, estimates of equilibrium perturbation height from Eq. 2.13 are shown in Table 2.1. Note that the values of h_o are sufficiently large to generate physically useful island dimensions. Electric fields of such high magnitude (10^9 *V/m*) can not be achieved at atmospheric pressure due to break-down of air. However, it is possible to apply such high fields at high vacuum of the order of 10^{-5} - 10^{-7} *torr* since the mean free path is about 5-100 *m* at this pressure and 250 ^oC. From the length scales shown Table 2.1, it follows that focused electric fields can be applied to a conducting surface to guide surface

diffusion and assemble nano- and micro-scale structures in any desired pattern and size distribution.

w (nm)	100	200	500	1000
h_o (nm)	5.7	22.8	143	570

Table 2.1: Equilibrium perturbation amplitude from Eq. 2.13 for $E = 10^9$ V/m and $\gamma = 1$ J/m^2

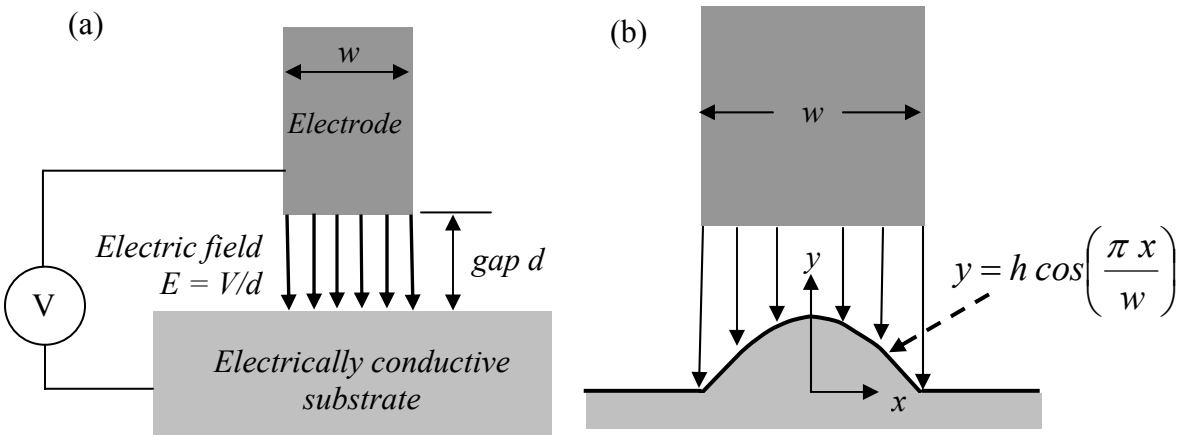

Fig. 2.1: Perturbation of a conductive substrate subjected to a localized electric field. (a) An electrode close to a conductive surface sets up an electric field in the gap. The two solids constitute a capacitor. (b) Stability of the flat configuration can be examined by considering incremental changes in free energy due to small sinusoidal surface perturbations.

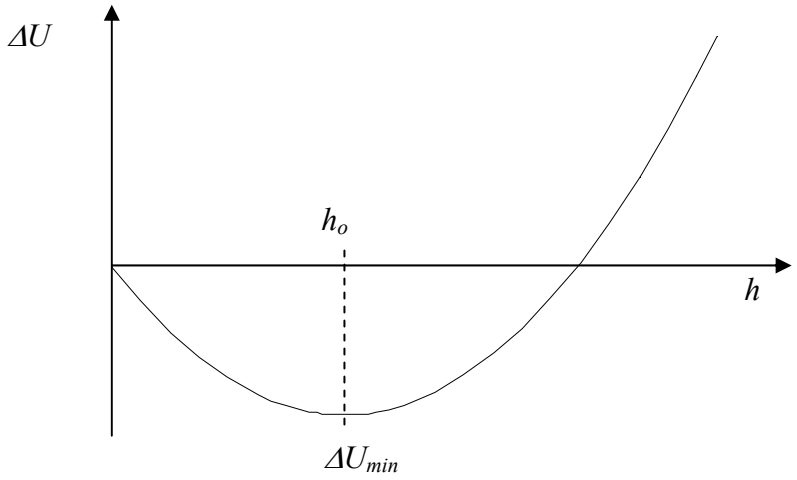

Fig. 2.2: Schematic illustration of energy variation (ΔU) with perturbation amplitude h. Note that ΔU is minimum at h_o given by Eq. 2.13, corresponding to the equilibrium perturbation height.

A similar analysis can be carried out for the 3-D case, which can be seen in Appendix A, of an electrode of square cross-section of side w, which results in an equilibrium perturbation height of

$$h_o = \frac{4\varepsilon_o V^2 w^2}{\pi^4 d^2 \gamma} \tag{2.14}$$

which differs from the 2-D case by a factor of $2/\pi$ only.

2.3 Stability of a conducting surface in a parallel plate capacitor

In contrast to the previous section where the electric field is localized to a small spot, consider a parallel plate capacitor configuration, illustrated in Fig. 2.3 in which surface evolves under a uniform electric field is examined. The two plates are separated

by a distance d, and a voltage V is applied between them, which sets up a uniform electric field $E = V/d$ between them. It is assumed that the length of the plates is large compared to their separation distance d, so that the edge effects can be neglected. Also, for the sake of simplicity, it is assumed that the lower plate has a much higher surface mobility than that of the upper plate, so that surface evolution is confined to the lower plate only. It is instructive to examine whether the initial flat configuration is stable under the applied uniform field, by considering the change in potential energy corresponding to a sinusoidal perturbation of wavelength λ shown in Fig. 2.3(b).

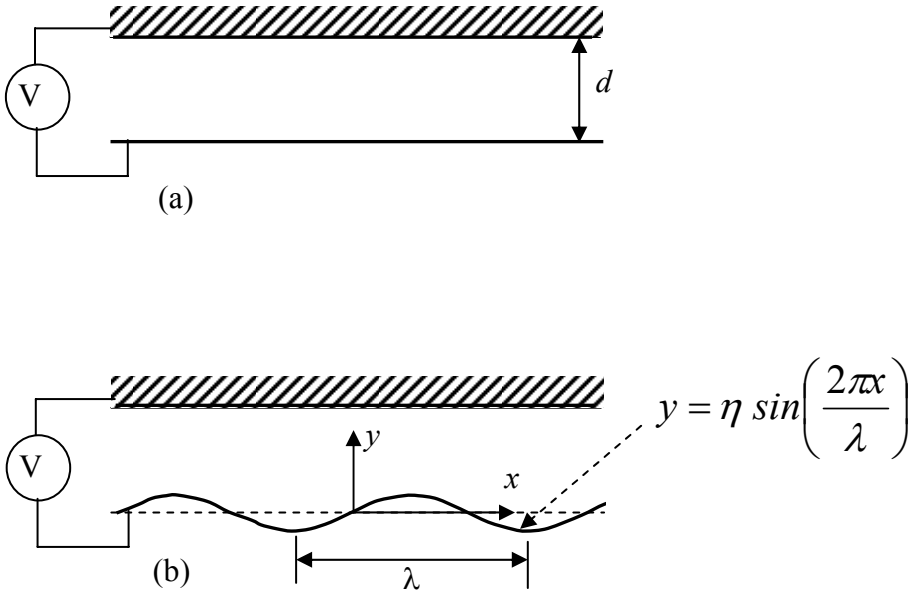

Figure 2.3: Electric field induced surface instability in a parallel plate capacitor. (a) Initial surface geometry. (b) Perturbed geometry of the surface.

The 2-D surface perturbation shown in Fig. 2.3(b) can be described as $y = \eta Sin\left(\frac{2\pi x}{\lambda}\right)$, with an amplitude η, and wavelength λ, The amplitude η is considered to be much smaller than the distance d between the plates. For the initial flat surface, the capacitance over one wavelength λ is given by:

$$C_1 = \frac{\varepsilon_o \lambda}{d}. \tag{2.15}$$

where ε_o is the free space permittivity. The capacitance over a length of λ in the perturbed configuration can be approximately evaluated is:

$$C_2 = \varepsilon_o \int_0^{\lambda} \frac{dx}{d - \eta\, Sin\ \frac{2\pi x}{\lambda}} \tag{2.16}$$

which can be approximated as:

$$C_2 \approx \frac{\varepsilon_o}{d}\left(1 + \frac{\eta^2}{2d^2}\right)\lambda \tag{2.17}$$

Hence, the change in the electric potential energy is given by:

$$\Delta U_E = -\frac{\varepsilon_o \lambda\, V^2 \eta^2}{4\, d^3} \tag{2.18}$$

The initial surface energy, U_1 over one wavelength is:

$$U_1 = \gamma\lambda \tag{2.19}$$

The corresponding quantity for the perturbed shape, U_2, can be evaluated as

$$U_2 = \gamma \int_0^{\lambda} \sqrt{1 + \left(\frac{dy}{dx}\right)^2} \sim \gamma \int_0^{\lambda} \left[1 + \left(\frac{dy}{dx}\right)^2 \Big/ 2\right] = \gamma\left[\lambda + \frac{\eta^2 \lambda^2}{\lambda}\right] \tag{2.20}$$

Thus the change in the surface energy is:

$$\Delta U_s = \frac{\pi^2 \gamma \eta^2}{\lambda} \tag{2.21}$$

The total change in the potential energy of the system due to the introduction of the sinusoidal perturbation is given by:

$$\Delta U = \left[\frac{\pi^2 \gamma}{\lambda} - \frac{\varepsilon_o \lambda V^2}{4 d^3} \right] \eta^2 \tag{2.22}$$

Note that, for a given set of parameters, the sign of the potential energy change depends on the value of the perturbation wavelength. The critical wavelength λ_c above which the perturbations are energetically admissible is obtained by setting $\Delta U = 0$ and can be expressed as:

$$\lambda_c = \sqrt{\frac{4 \pi^2 d \gamma}{\varepsilon_o E^2}} \tag{2.23}$$

Perturbations of wavelength greater than λ_c have an energetic driving force to grow, whereas those with shorter wavelengths are expected to decay in time.

Thus, in contrast to the case of focused electric field considered in the previous section, even a uniform electric field can lead to surface roughening and island growth. This situation is similar to strain induced island growth in epitaxial films where the surface energy and the elastic energy compete with each other. In the current problem, the reservoir of elastic energy in the solid is replaced with a reservoir of electric field energy in the space outside the solid. For $E = 10^9$ *V/m*, $\gamma \sim 1$ *J/m*^{2}, $\varepsilon_o = 8.85 \times 10^{-12}$ *C*^{2}*/Nm*^{2}, typical values of (d, λ_c) can be seen in Table 2.2. Thus, the above analysis suggests that, by choosing appropriate values for d and E, it should be possible to drive a self-assembly process to create surface islands on conducting surfaces at micron to

nanometer scale. A similar analysis for a 3-D perturbation which is sinusoidal in both in-plane directions results in exactly the same value of the critical wavelength. The 3-D analysis is presented in Appendix B.

d (nm)	10	100	500	1000
λ_c (nm)	210	670	1490	2100

Table 2.2: Critical wavelength from Eq. 2.23 for $E = 10^9$ V/m, $\gamma = 1$ J/m^2 and $\varepsilon_o = 8.85 \times 10^{-12}$ C^2/Nm^2

2.4 Kinetics of surface diffusion under external electric field

The preceding two sections discussed the energetics of surface perturbations and demonstrated the driving force for a surface to evolve under the influence of an external electric field. As discussed earlier, surface diffusion is the mechanism which enables shape evolution. In this section, the kinetics of surface diffusion is considered and the governing equation for the time evolution of a surface is obtained.

Freund (1995) discussed the problem of evolution of waviness on the surface of a strained elastic solid, where surface diffusion is driven by the competition between the elastic energy and the surface energy. By following a similar procedure with an additional electrostatic field energy term, a surface chemical potential can be defined as follows. Consider a segment of the surface shown in Fig. 2.4, that represents a part of an evolving conducting surface under an electric field. For example, this can be the evolving surface under the electrode in Fig. 2.1 or that in the parallel plate capacitor in Fig. 2.3. The space outside the solid stores electric field energy of density U_E. One might consider

the stored elastic energy density U_e of the solid as well, in case the solid is strained. The free energy of the system consists of the elastic energy, the electrostatic field energy and the surface energy. If B is the volume of the solid, B' is the volume outside the solid and S is the surface, then the free energy F, as a function of time t can be written as

$$F(t) = \int_B U_e \, dB + \int_{B'} U_E \, dB' + \int_S \gamma \, dS \tag{2.24}$$

where γ is the surface energy per unit area. The surface evolves with a normal velocity V_n. If there is no exchange of energy between the system (consisting of the elastic solid, its surface, the surrounding space filled with the electric field and the power source that maintains a constant potential difference between the electrodes) and its surroundings, the rate of change of free energy can be simply written as the time derivative of Eq. 2.24 as

$$\dot{F}(t) = \int_S \left[U_e - U_E - \kappa \gamma\right] V_n \, dS \tag{2.25}$$

where κ is the sum of the principal curvatures of the surface. From Eq. 2.25, The local electro-elastic chemical potential (per atom) can be defined as

$$\mu = \left[U_e - U_E - \kappa \gamma\right] \Omega \tag{2.26}$$

where Ω is the atomic volume. The gradient in the chemical potential μ is the energetic driving force for surface evolution. Matter flows from regions of higher chemical potential towards regions of lower chemical potential. In the absence of any external electric field or any applied strain field the chemical potential is simply a function of the curvature of the surface. The normal velocity of the surface can be found by setting the diffusion flux to be proportional to gradient in chemical potential and invoking the principle of conservation of mass and is given by

$$V_n = \frac{\delta D \, \Omega}{kT} \nabla^2 \mu \tag{2.27}$$

Here δD is surface diffusivity (D) times a characteristic thickness (δ) over which diffusion is supposed to take place. k is the Boltzman constant, T is the absolute temperature and ∇^2 is the Laplacian operator on the surface. Eq. 2.27 combined with Eq. 2.26 provides the governing equation for surface evolution, which needs to be solved along with appropriate initial and boundary conditions.

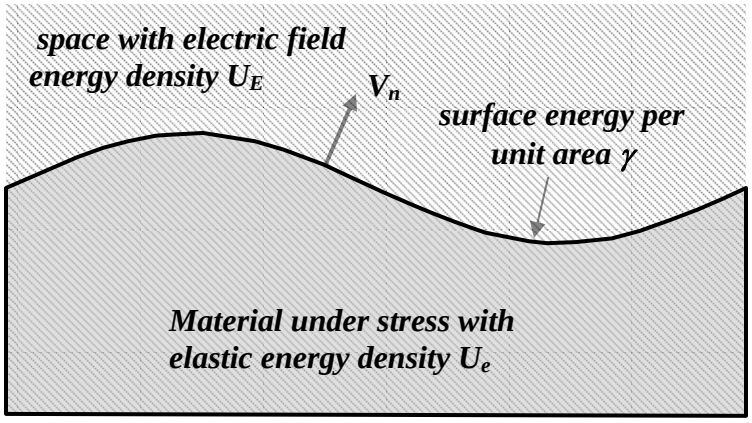

Figure 2.4: Schematic illustration of a conductive solid with an evolving boundary in the presence of an electric field outside it. The surface normal velocity is V_n.

As an example, Eq. 2.27 can be used to examine the kinetics of the growth of the perturbation shown in Fig. 2.3(b), in which the electric field along the surface can be approximated as

$$E(x) = \frac{V}{d - y(x)} \tag{2.28}$$

where $y(x) = \eta \sin(2\pi x/\lambda)$ is the shape of the perturbation. Ignoring the elastic energy term, the chemical potential of the surface becomes

$$\mu(x) = \left[-\frac{\varepsilon_o V^2}{2(d - y(x))^2} - \gamma\, y''(x) \right] \Omega \approx \left[-\frac{\varepsilon_o V^2}{2d^2} \left(1 + \frac{2y(x)}{d} \right) - \gamma\, y''(x) \right] \Omega \quad (2.29)$$

where the approximation is valid for $\eta/d << 1$. For small slopes, the normal velocity V_n and the curvature κ can be approximated as dy/dt and d^2y/dx^2, respectively. Hence, Eq. 2.27 reduces to

$$\frac{dy}{dt} = \frac{\delta D \Omega}{kT} \frac{d^2 \mu}{dx^2} = \frac{d\eta}{dt} Sin \frac{2\pi x}{\lambda} \quad (2.30)$$

Combining Eq. 2.29 and Eq. 2.30

$$\frac{d\eta}{dt} = \left(\frac{4\pi^2 \varepsilon_o V^2}{\lambda^2 d^3} - \frac{16\pi^4 \gamma}{\lambda^4} \right) \eta \quad (2.31)$$

Solution to Eq. 2.31 yields an evolution equation for the perturbation amplitude η as

$$\eta = \eta_o \exp \left\{ \frac{\delta D \Omega}{kT} \left[\frac{4\pi^2 \varepsilon_o V^2}{\lambda^2 d^3} - \frac{16\pi^4 \gamma}{\lambda^4} \right] t \right\} \quad (2.32)$$

where η_o is the initial perturbation amplitude. The coefficient of t in the exponent, denoted by $r(\lambda)$ given by Eq. 2.33, can be regarded as the growth rate of the perturbation of wavelength λ.

$$r(\lambda) = \left[\frac{4\pi^2 \varepsilon_o V^2}{\lambda^2 d^3} - \frac{16\pi^4 \gamma}{\lambda^4} \right] \quad (2.33)$$

The critical wavelength λ_c in Eq. 2.23 can be recovered by setting $r(\lambda) = 0$. A non-dimensional plot of $r(\lambda)$ as a function of the wavelength is shown in Fig. 2.5. The

wavelength of the fastest growing perturbation wavelength can be calculated by setting $\frac{dr(\lambda)}{d\lambda} = 0$ and is given by

$$\lambda_m = \sqrt{\frac{8\pi^2 d\gamma}{\varepsilon_o E^2}} = \sqrt{2}\,\lambda_c \tag{2.34}$$

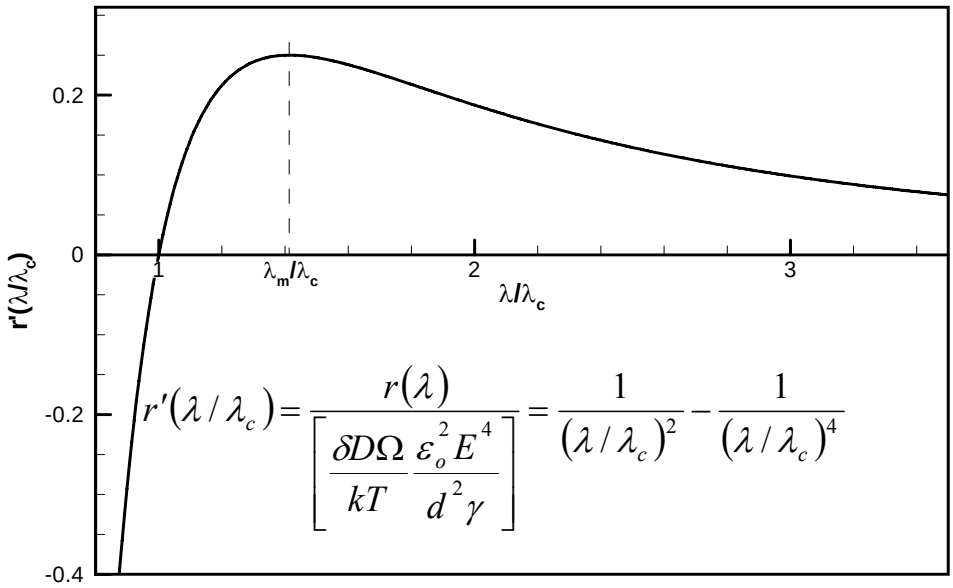

Figure 2.5: Non-dimensional perturbation growth rate as a function of its wavelength, showing the fastest growing mode.

The characteristic time for the fastest growing mode can be defined as

$$\tau = \frac{2\,kTd^2\gamma}{\delta D\,\Omega\,\varepsilon_o^2 E^4} \tag{2.35}$$

τ can be interpreted as the time for the perturbation amplitude to grow by a factor of *e*. It is instructive to examine the magnitude of τ for gold at a temperature of 250 ^oC , 275 ^oC and 300 ^oC under an applied electric field of 5 X 10^8 V/m and a gap *d* of 0.2 μm which are typical parameters for the experiments to be described in the next chapter. The surface diffusivity of many FCC metals can be described by (Philibert, 1991),

$$\begin{aligned} D &= 7.4 \times 10^{2}\, exp\left(-15\, T_M / T\right) cm^2/s \quad for \quad T > 0.75\, T_M \\ D &= 14 \times 10^{-2}\, exp\left(-7\, T_M / T\right) cm^2/s \quad for \quad T < 0.75\, T_M \end{aligned} \tag{2.36}$$

where T is the absolute temperature and T_M is the melting temperature of the metal. Characteristic times for the above values, along with δ = 0.5 nm, Ω = (0.5 nm)^3, T_M = 1338 K are shown in table 2.3.

As expected, the characteristic growth time is highly sensitive to temperature. The temperature dependence of τ on temperature is further illustrated in Fig. 2.6. It is clear that, from the point of view of fabricating nano/micro islands by means of electric fields, the processing times are expected to be reasonably short to be practical.

Temp. (^{o}C)	200	225	250	275	300
τ (hours)	14	5.4	2.3	1.1	0.5

Table 2.3: Temperature versus characteristic time for perturbation to grow.

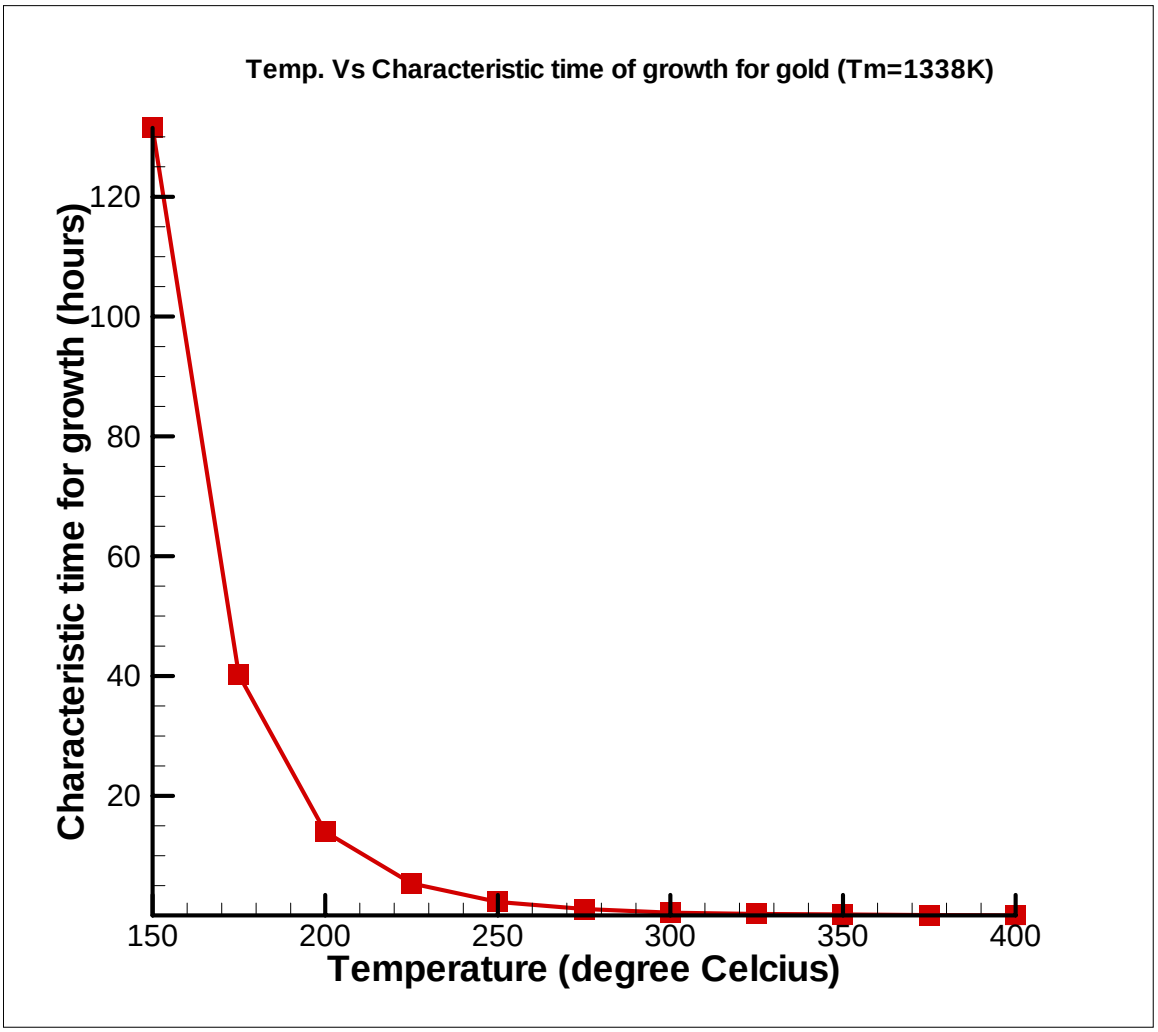

Figure 2.6: Plot of characteristic time for the instability to grow versus temperature for gold with melting temperature of 1338 K.

2.5 Kinetics of surface evolution at the edge of a parallel plate capacitor

In the previous sections, surface diffusion driven by a uniform electric field was discussed, while ignoring the edge effects. However, in an experimental configuration in which two flat electrodes are brought close each other, edge effects are inevitable and can be dominant as well. In order to understand surface evolution at the edges, consider a semi-infinite parallel plate capacitor geometry, which contains a fringe field, as illustrated in Fig. 2.7(a). It turns out, as will be discussed in subsequent chapters, that the fringe field plays a major role in surface evolution compared to the instability induced by the uniform field in the interior of the capacitor. The surface evolves quite differently at the edges where the field is not uniform as compared to the sections where the applied field is uniform. Surface evolution at the edge of a semi-infinite parallel plate capacitor in the presence of a fringe field is considered in this section.

Although the width of the electrode in any experiment in finite, if it is much greater than the gap, the top plate can be idealized to be semi-infinite, extending over $-\infty < x \leq 0$ & $y = d$, whereas the bottom electrode extends over $-\infty < x < \infty$ & $y = 0$. When a voltage is applied between the two plates, the electric field is zero well outside the top plate at $x/d >> 1$, thus there is no driving force for diffusion there. In the interior of the capacitor, $x/d << 1$, the electric field is uniform and the only driving force for surface evolution arises from the surface instability described in the previous section. However, near the edge of the top plate ($x/d \sim 1$), the fringe field causes a strong gradient in the electric field at the surface of the bottom plate, resulting in a driving force for surface diffusion. It is useful to calculate the surface normal velocity profile within the fringe

field, which can serve as a reference for interpreting the experimental results, which will be discussed in a subsequent section.

The solution for the electric field near the edge of a finite parallel plate capacitor was first given by Maxwell (1879), which was further developed by Rogowski (1923). A summary of the solution is given by Cobine (1941), which will be utilized here. With reference to Fig. 2.7(a), let the potential of the bottom plate be zero, that of the top plate be V_o and the potential at a point in space be $V(x,y)$. Then, if the non-dimensional potential is defined as $\psi = \pi V/V_o$ and its conjugate harmonic potential is denoted by ϕ, the fringe field is given by

$$x = \frac{d}{\pi}\left[1 + \phi + e^{\phi}\ cos\ \psi\right], \qquad y = \frac{d}{\pi}\left[\psi + e^{\phi}\ sin\ \psi\right] \tag{2.37}$$

Note that, being conjugate harmonic functions, φ and ψ satisfy the Cauchy-Riemann equations

$$\frac{\partial \phi}{\partial x} = \frac{\partial \psi}{\partial y}, \frac{\partial \phi}{\partial y} = -\frac{\partial \psi}{\partial x} \tag{2.38}$$

Now, the electric field E along the bottom plate ($y=0$) is

$$E = -\frac{\partial V}{\partial y} = -\frac{V_o}{\pi}\frac{\partial (V\pi/V_o)}{\partial y} = -\frac{V_o}{\pi}\frac{\partial (\psi)}{\partial y} \tag{2.39}$$

Along the surface of the bottom plate, where $\psi = 0$, Eq. 2.37 becomes

$$x = \frac{d}{\pi}\left[\phi + 1 + e^{\phi}\right] \tag{2.40}$$

Differentiative Eq. 2.40 with respect to x,

$$1 = \frac{d}{\pi}\left[\frac{\partial \phi}{\partial x} + e^{\phi}\frac{\partial \phi}{\partial x}\right] \tag{2.41}$$

Combining Eq. 2.41 and the Cauchy-Riemann equations 2.38,

$$\frac{\partial \phi}{\partial x} = \frac{\partial \psi}{\partial y} = \frac{\pi}{d\,(1 + e^{\phi})} \tag{2.42}$$

By substituting Eq. 2.42 in Eq. 2.39, the electric field near the surface of the bottom plate can be expressed as

$$E\,(x, y = 0) = -\frac{V_o}{d\,(1 + e^{\phi})} \tag{2.43}$$

The negative sign indicates that the field points in the negative y direction. By using Eq. 2.59 in Eq. 2.43, the surface evolution equation becomes,

$$\frac{dy}{dt} = \frac{\pi^2 \varepsilon_o E_o^2 \delta D \Omega}{d^2 kT}\left[\frac{e^{\phi} - 3e^{2\phi}}{\left(1 + e^{\phi}\right)^6}\right] \tag{2.44}$$

where ϕ is given by Eq. 2.41. Note that γ does not appear in Eq. 2.43 because the surface is initially flat. Hence, the above evolution equation is valid only when the electric field is turned on and is approximately valid subsequently while the curvature contribution to the chemical potential is small compared to the electric field term, The magnitude of the electric field is plotted in Fig. 2.7b and the initial surface velocity (Eq. 2.44), normalized with a reference velocity V_r, is plotted in Fig. 2.7(c). V_r is defined as

$$V_r = \frac{\pi^2 \varepsilon_o E_o^2 \delta D\,\Omega}{d^2 kT} \tag{2.45}$$

As seen in Fig. 2.7(c), the surface velocity and thus the driving force for diffusion are highest in the gradient or fringe field region, resulting in a peak just inside the capacitor edge and a valley outside. However, the main limitation of this analysis is that it does not predict the surface velocities following surface perturbation, when surface energy term in the chemical potential becomes significant. To determine surface

evolution over experimentally relevant time scales, it would be necessary to solve the evolution equation 2.44 numerically, which is discussed in a subsequent chapter.

2.6 Summary

- In summary, the stability of a conducting surface was analyzed in this chapter. The influence of an external electric field on conducting surfaces is considered in this chapter. By considering the energetics, it was demonstrated that a localized electric field induces a configurational force on a conducting surface to evolve and to form micro and nano-scale islands.
- External fields can lead to surface evolution in two ways: an instability in a uniform field and evolution driven by a gradient in the magnitude of the electric field.
- For instability induced by a uniform field, there is a critical perturbation wavelength, above which the perturbations are energetically admissible.
- A surface chemical potential can be defined in the presence of an external electric field and a surface evolution equation can be obtained in terms of the chemical potential. The critical wavelength and the fastest growing perturbation wavelength can be calculated by considering the kinetics of surface evolution.
- Initial surface evolution velocity at the edge of a parallel plate capacitor is calculated by utilizing the Maxwell-Rogowski fringe field solution, which can be used to interpret experimental observations

The foregoing analysis serves as the motivation for the experimental effort to demonstrate that surface evolution can indeed be induced and controlled by an electric field and micro and nano-scale islands can be grown, which will be described in the next chapter.

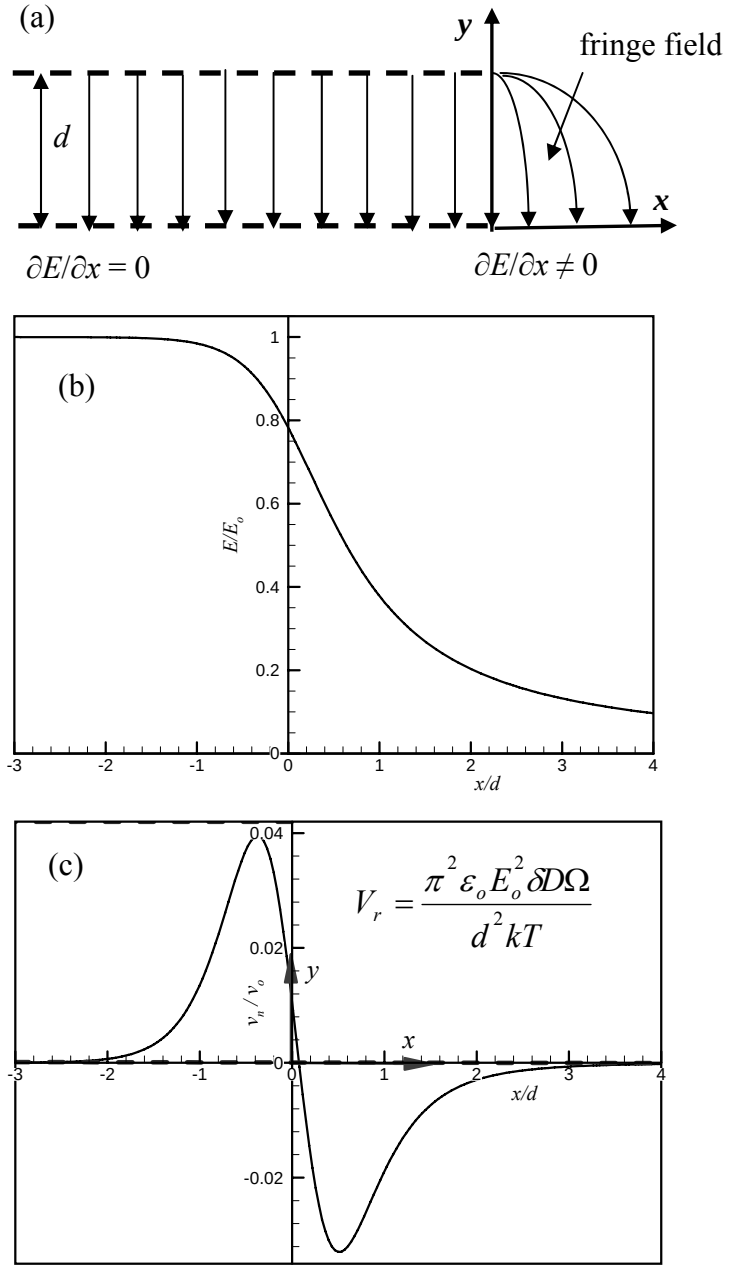

Figure 2.7:(a) Schematic illustration of a finite parallel plate capacitor, approximating the experimental geometry. Both plates extend to infinity in the negative x direction. The top plate ends at x = 0 and the bottom plate extends to infinity in positive x direction. The field is uniform in the interior. Near the edges (fringe field), the field gradient is maximum, providing highest driving force for surface diffusion. (b)The magnitude of electric field near the edge of the finite plate. (c) A plot of the surface normal velocity V_n due to the fringe field induced surface diffusion.

Chapter 3

Experimental Investigation

3.1 Introduction

Although there have been discussions in the literature of the influence of electric field on surface diffusion, experimental observations have so far been limited to STM tip-surface interactions (Avouris, 1995; Li et al. 1996; Dulot et al. 2000; Murphy et al. 2003), mainly as a means for single atom manipulation. There have been no systematic attempts to study the phenomenon and to exploit it as a technique to create surface features with spatial and size control. In the preceding chapter, it was demonstrated that an electric field can lead to surface evolution in two ways: (i) a uniform field can destabilize an initially flat surface and lead to micro and nano-scale island formation, similar to strain driven self assembly; (ii) a gradient in the electric field, such that in a fringe field, can provide chemical potential gradient to drive surface diffusion. Further, it was shown that, in principle, by applying sufficiently strong electric fields and carrying out the experiment at high enough temperature, islands of physically useful dimensions (a few hundreds of nanometers) can be realized within experimentally realistic time scales.

This section presents an experimental investigation to realize the above predictions and to demonstrate electric field induced continuum surface diffusion at micron and sub-micron scales. To achieve this goal, an experimental setup has been designed and built, which will be explained in detail in a subsequent section. Also,

appropriate samples were designed and fabricated using various micro-fabrication techniques such as photo-lithography, electron beam evaporation, reactive ion etching, etc, which will be described in detail. The experimental results are interpreted with reference to the analyses described in the preceding sections. The eventual goal of this effort is to develop a fabrication technique for small scale ordered surface features on conducting materials.

3.2 Sample design and fabrication

As demonstrated in section 2.2, the magnitude of the electric field necessary to get sub-micron sized islands is of the order of 10^8 *V/m* to 10^9 *V/m* or 0.1 *V/nm*-1 *V/nm*. In order to apply such high fields, the two electrodes have to be apart by no more than a few hundred nanometers. Since air at atmospheric pressure breaks down around 10^6 *V/m*, the experiments need to be carried out at sufficiently high vacuum conditions. High vacuum condition also minimizes oxidation of the electrode surfaces at the elevated temperatures at which the experiments are carried out. In addition, most of the dielectrics break down between 10^6 *V/m* and 10^7 *V/m*; hence, it must be ensured that the applied electric field is confined to the space between the electrodes only and does not pass through any part of the patterned dielectric layer that maintains the desired gap of a couple hundred nanometers between the electrodes. Gold was chosen as the sample material, primarily for its greater resistance to oxidation under high vacuum conditions compared to other conductors. Titanium was chosen as the material for the other electrode to apply the electric field. Since the melting point of titanium (1660 ^oC) is substantially higher than that of gold (1064 ^oC), the latter is expected to undergo surface diffusion more readily

than titanium. Hence the gold electrode is the surface of interest in the experiments. The sample and electrode geometry was designed while taking the above constraints into consideration.

3.2.1 Design and fabrication of electrodes

The basic sample arrangement is illustrated in Fig. 3.1. Fig. 3.1(a) shows the geometry of the gold surface on a glass substrate; the thickness of the gold line is 200 *nm* – 225 *nm* and width is varied between 1 μm and 100 μm. The length of the gold line is several millimeters, much larger than the width. The glass substrates are 12.5mm squares and 1 *mm* in thickness. Each gold line is flanked on either side by an alumina film, whose thickness is about 200 *nm* greater than that of the gold line [Fig. 3.1(a)]. The sample consists of several parallel gold lines, separated by alumina films, which are joined at one end and connected to the terminal of a power supply. The greater height of the alumina film compared to that of the fold film serves the purpose of maintaining a gap of desired height between the gold and the titanium electrodes, which will be referred to as the bottom and the top electrodes respectively in this discussion. The top electrode is simply a patterned titanium film on a second glass plate, as illustrated in Fig. 3.1(b). The film thickness is approximately 200 *nm*. The two glass patterned glass plates are then assembled as shown in Fig. 3.1(c), where the top and the bottom electrodes are nearly perpendicular to each other. The alumina film acts as a "spacer block" and maintains a gap of about 200 *nm* between the gold and the titanium electrodes. When the electrodes are connected to a voltage source that applies a potential difference V between them, the resulting electric field is confined to the overlapping regions of the gold and the titanium

lines only. An end-view of the assembled sample is shown in Fig. 3.1(d). Note that the region of overlap between a gold line and a titanium line acts like a parallel plate capacitor, whose length (equal to the width of the titanium line) is much greater than the gap height (~ 200 *nm*). Also, the gold film experiences the fringe field near the two edges of the titanium line. Some of the gold and titanium lines are not connected to the voltage source by design; these lines act as control electrodes in order to isolate the effect of the electric field.

The microfabrication process to prepare the gold electrode is illustrated in Fig. 3.2. A detailed description of the processing details is given in Appendix C. In order to promote adhesion between gold and glass, a 10 *nm* thick titanium layer is deposited on the sample prior to gold evaporation, although this step is not shown in Fig. 3.2. A micrograph of a portion of the gold electrode is shown in Fig. 3.3(a). A terminal wire is attached to the gold film with conducting silver epoxy (Cotronics Inc., Brooklyn, NY), which is stable up to 650 ^{o}C.

Fabrication of the titanium electrode is very similar to that of the gold electrode and simpler, because there is no aluminum oxide step. A micrograph of a portion of the top glass plate is shown in Fig. 3.3(b). Sample fabrication was carried out in Brown University Micro-electronics facility and the Harvard Nano-fabrication facility.

The peak-peak roughness of the electrode surfaces is measured to be about 6 *nm*, which is much smaller than the electrode spacing. However, long wavelength waviness of the glass plates prevents contact of the titanium electrodes with the alumina film everywhere. Intimate contact is realized only in limited regions of the sample surface. Growth of islands, to be described later, is observed in these regions of good contact.

Following assembly, the sample is placed inside the process chamber, which will be discussed in the next section.

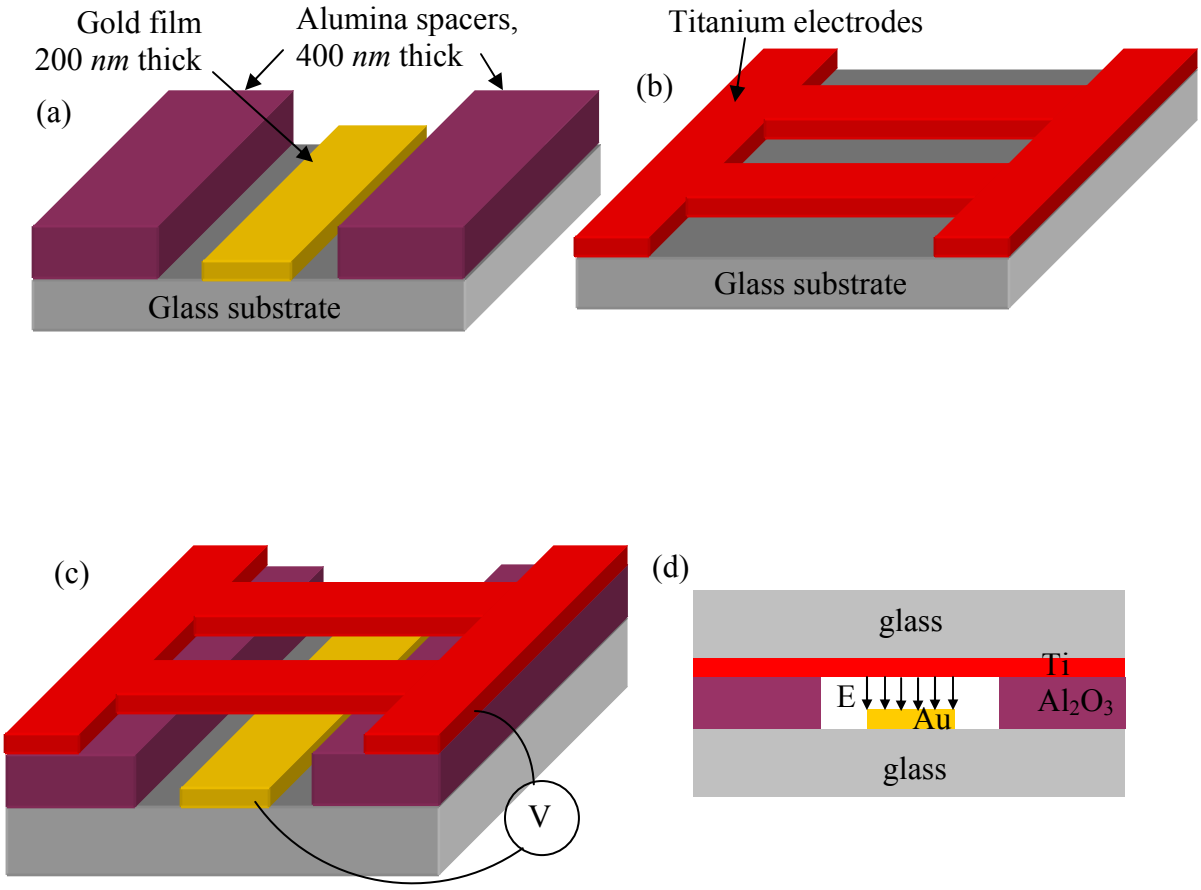

Figure 3.1: Schematic illustration of the sample design to study electric field induced surface diffusion. (a) A 200 nm thick gold film on a glass plate is flanked by 400 nm thick alumina films, which act as "spacers" to maintain a distance of 200 nm between the top titanium electrodes and the bottom gold electrode. (b) The top titanium electrodes are patterned on the top glass plate. (c) The plate in (b) is turned up side down and brought into contact with alumina spacers in (a). The top glass plate is not shown for clarity. (d) The cross-section of the assembled sample, carrying the electric field between the electrodes. Note that none of the dielectrics in the sample are subjected to the electric field in this design to prevent their breakdown.

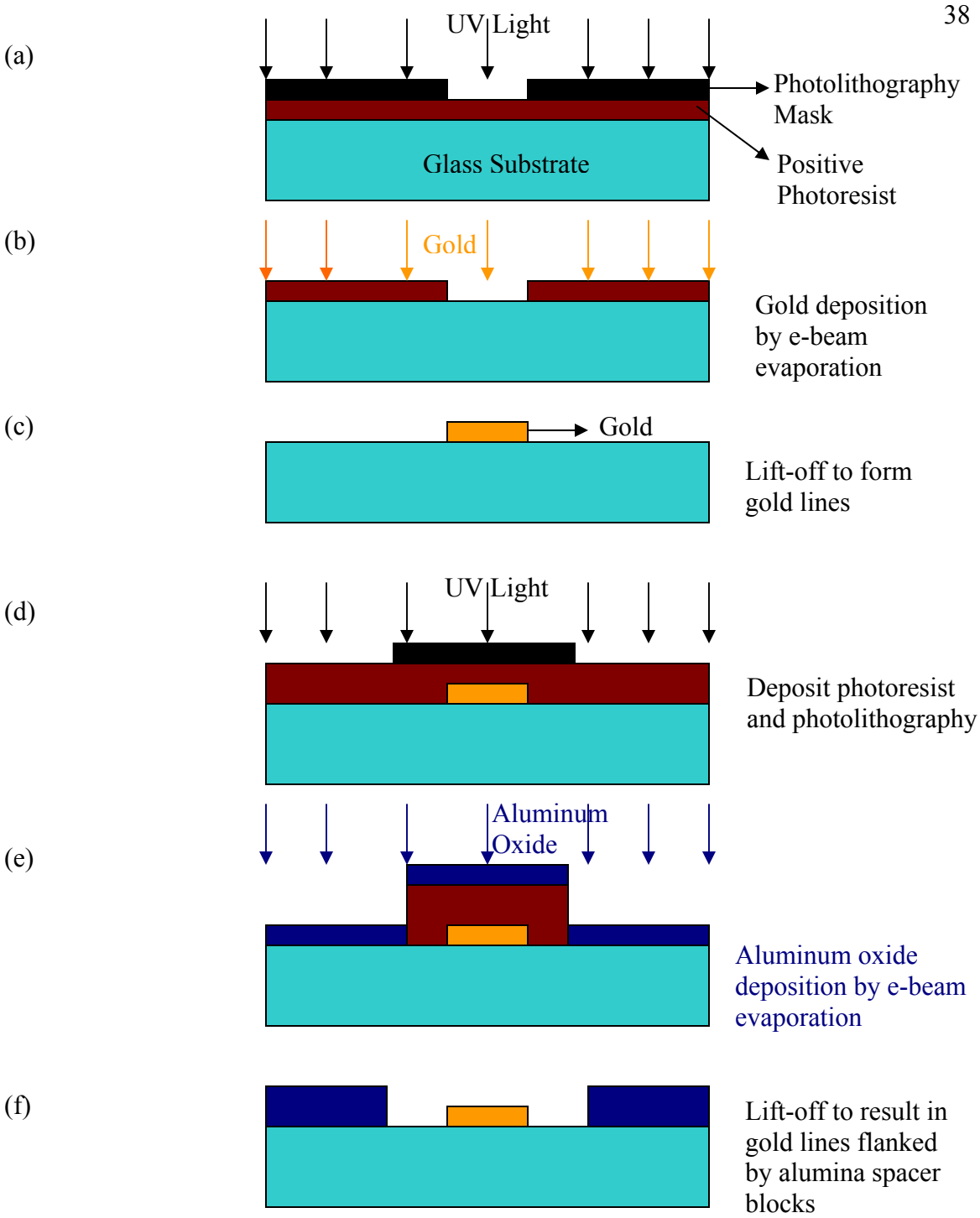

Figure 3.2: Schematic of sample fabrication process for lower gold electrode sample, (a) Photolithography is carried out for a positive photoresist on a glass substrate (b) Thin film of gold is deposited using E-beam evaporation (c) Photoresist is etched away and thin gold film is left on the glass substrate (d) Positive photoresist is spin coated and photolithography is carried out (e) Aluminum oxide is deposited on the sample using E-beam evaporation (f) Final sample with gold sandwiched between two aluminum oxide spacers

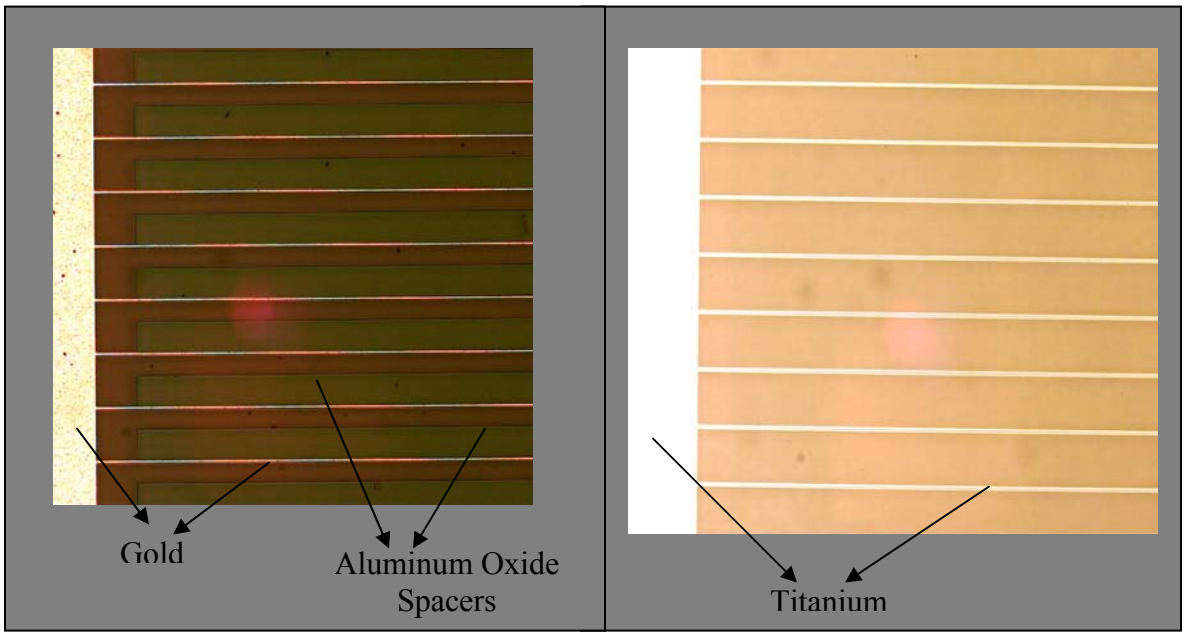

(a) (b)

Figure 3.3: Optical micrographs of the samples (a) Lower sample with gold electrodes sandwiched between aluminum oxide spacers (b) Upper sample with titanium electrodes.

3.3 Process chamber

As discussed earlier, the magnitude of electric field that needs to be applied to get significant surface diffusion and island formation is of the order of $10^8 V/m$ to 10^9 V/m. At these values of the electric field, the atmospheric air breaks down and causes sparking between the upper and the lower electrodes. Hence the experiments are carried out in sufficiently high vacuum conditions. Moreover, the experiments are conducted at an elevated temperature to permit surface diffusion; high vacuum conditions reduce oxide formation on the electrode surfaces at these high temperatures. Through the course of the investigation, after carrying out experiments at several temperatures, it was determined that a temperature range of 250-300 ^oC is ideal, where the surface diffusivity is high

enough to form micro and nano-scale islands driven by the electric field in reasonable time scales, while at the same time not lead to excessive grain boundary grooving in the same time scales. Thus, the process chamber is essentially a vacuum chamber, which holds a heating chamber and an arrangement to apply electric field. It is also necessary to monitor the electric current between the electrodes, which remains zero under normal operation, but increases in case of any unintended breakdown of the vacuum between the electrodes.

The process chamber consists of a Pyrex cylinder, 370 *mm* long and 305 *mm* in diameter. Viton Gaskets (Greatglas Inc.), 305 *mm* in diameter are mounted on each end of the Pyrex cylinder. The chamber rests on a stainless steel base plate, which can accommodate several feedthroughs. The experiments use the following feedthroughs:

- Two 12 *V* electrical feedthroughs (BOC Edwards, Model 6EK25) for the band heater used to heat the sample.
- One electrical feedthrough (BOC Edwards, Model TL8K25) for applying voltage between the electrodes.
- One K-type thermocouple feedthrough for monitoring sample temperature (BOC Edwards).

The top of the chamber is covered with a similar stainless steel plate. The chamber operates at around $\sim 10^{-7}$ *torr*, which also helps reduce oxidation of the electrodes at elevated temperatures. Through the course of the experiments, it was found that such a vacuum can support an electric field of the order of 10^{9} *V/m*. The chamber vacuum is maintained by a mechanical pump (BOC Edwards, Model: E2M1.5) and a turbo pump

(BOC Edwards, Model: EXT70H). Photographs of the process chamber and the sample/heater assembly are shown in Fig. 3.4.

In order to increase surface mobility, the experiments are carried out over a temperature range of 220 ^{o}C – 300 ^{o}C. During each experiment, resistance and current between the electrodes are monitored continuously to ensure that the former remains "infinite" (above the upper limit the measuring instrument) and the latter remains zero and to ascertain that a short circuit or breakdown does not develop. The sample assembly is kept inside a slot cut in a macor housing. Macor is a machinable ceramic, which facilitates fabrication and also withstands high temperatures. The geometry of the macor block, along with the sample assembled in it, is illustrated in Fig. 3.5. A band heater, which surrounds the macor block, is used to heat the sample. The sample temperature is monitored with a thermocouple, which contacts the glass plate that contains the titanium electrode on it. The sample temperature is maintained at the desired set point by controlling the power to the heater through an Omega CN370 (Omega Inc.) micro controller.

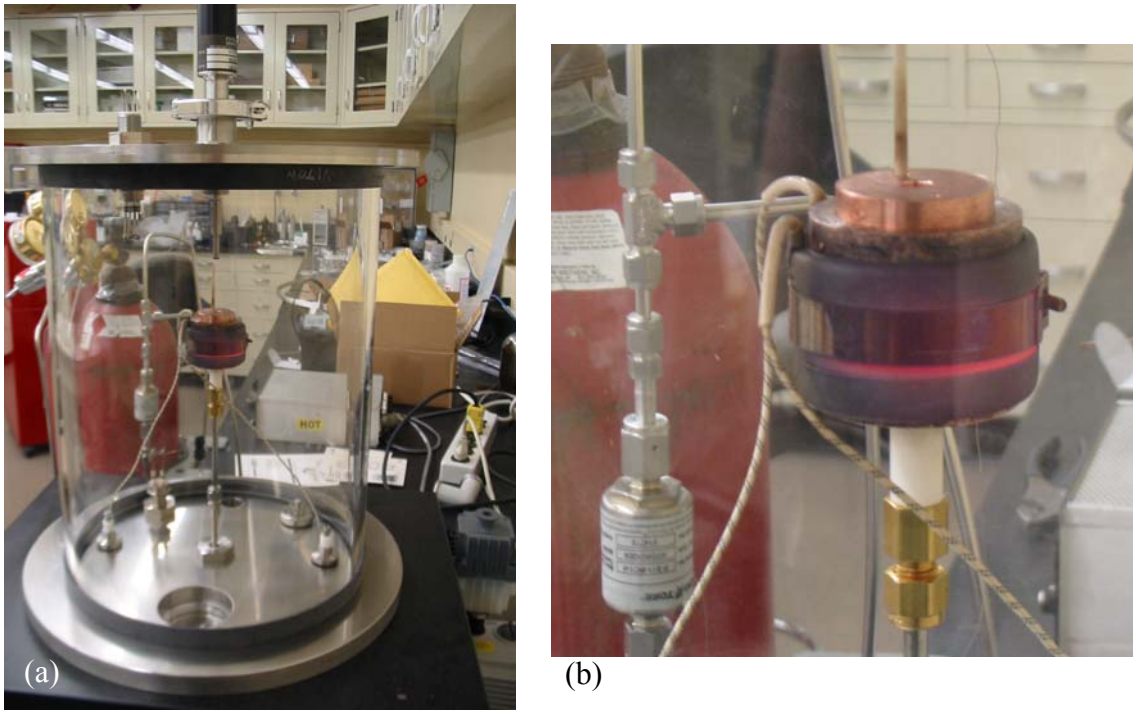

Figure 3.4 (a) A photograph of the process chamber constructed for the current experiments. (b) A close up view of the sample housing along with a heating element around it.

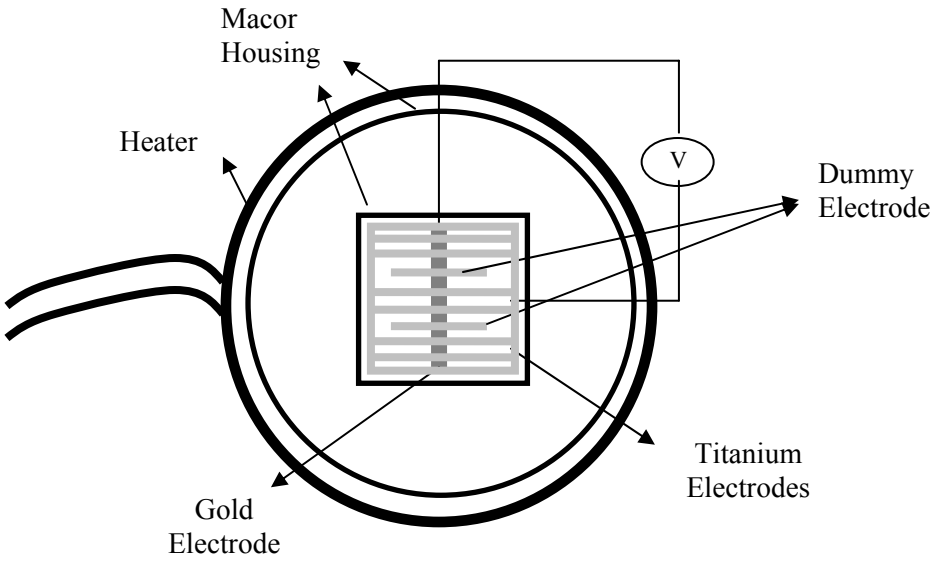

Figure 3.5: Schematic Illustration of the setup with the sample in the middle of a macor fixture which is heated on the outside by a nozzle-band heater.

3.4 Experimental results

The experiments were carried out inside the process chamber as described in previous sections. Before the experiment, an image of the gold test surface was obtained using tapping mode Atomic Force Microscope (DI Instruments Dimension 3100 AFM). The image of the gold surface can be seen in Fig. 3.6(a) which shows the grain structure. Fig. 3.6(b) shows a line-scan of height variation. The grain size in this polycrystalline film varies between 30 *nm* and 100 *nm*. The peak to peak roughness of the gold surface is approximately 6 *nm*. It will be seen later that the in-plane dimensions of the islands induced by the electric field are substantially larger than the grain size.

Since the width of the electrode is much larger than the gap in most experiments, each edge of the overlap area between the electrodes is well approximated by the illustration in Fig. 3.1 (c). The field is uniform over most of the electrode area, except near the edges where a fringe field exists. Hence, most of the activity in the experiments is expected near the edges, where the sample surfaces were imaged with an Atomic Force Microscope (AFM) after each experiment. Based on the width of the titanium electrode, the experiments can be grouped into three categories.

1. Large electrode size, i.e., electrode width greater than 20 μm..
2. Medium electrode size, i.e., electrode width ~ 10 μm.
3. Small electrode size, i.e., electrode width smaller than 4 μm.

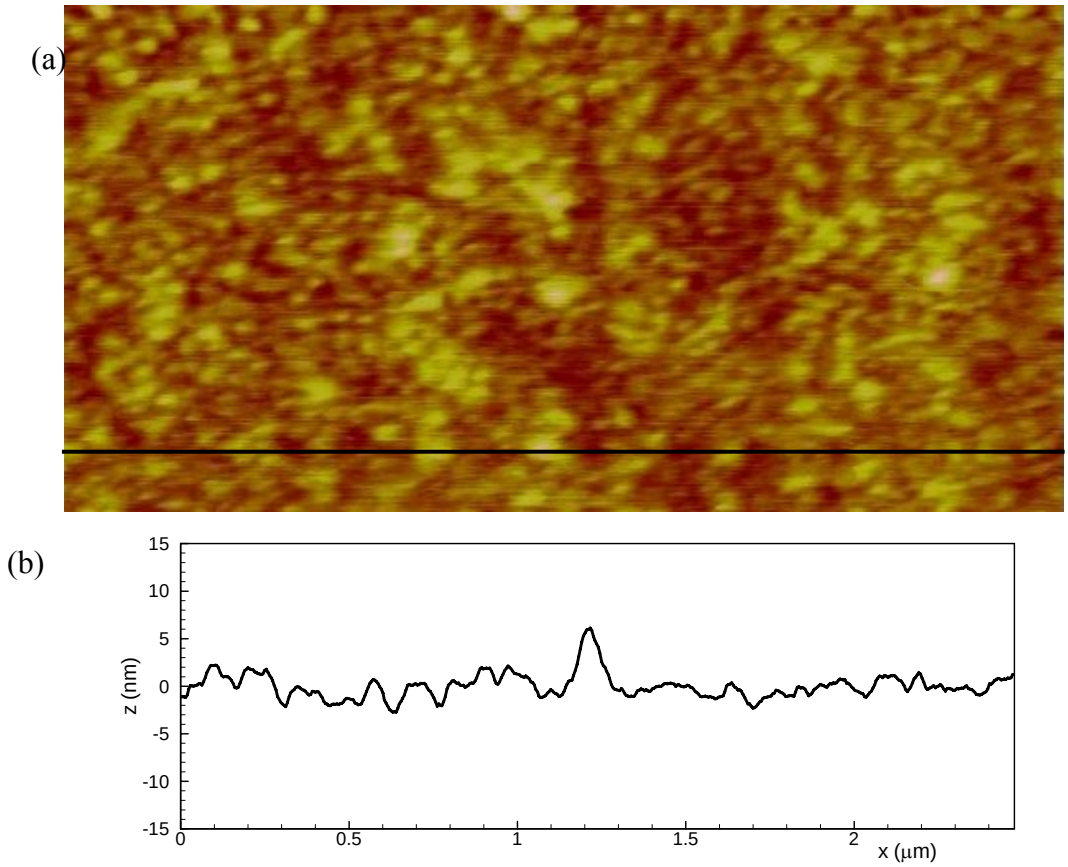

Figure 3.6: Grain structure of gold film before the experiment, (a) Showing grain size variation between 30 nm to 100 nm. (b)Height variation along a line is shown at the bottom. The peak to peak roughness is approximately 6 nm. In-plane scale bar for the figure is provided by the abscissa of the plot at the bottom.

3.4.1 Large electrode size (> 20 μm)

As discussed in previous chapter *(Section 2.4.1)*, due to the presence of the electric field gradient in the fringe field, the driving force for material to diffuse over the

surface is greatest at the edges of the electrode. Hence, it is expected that there would be significant surface diffusion near the edges of the electrode, which correlates very well with the experimental observations in the experiments with the electrode width larger than 20 μm. As shown in Fig. 3.7(a), the AFM scan of the areas under the electrode shows two bands of islands at the two edges of the electrode. The electrode width in this experiment was about 25 μm, and it was carried out at 280 ^{o}C for 4.5 hours. The magnitude of the applied electric field was $5x10^{8}$ V/m. The line scan in Fig 3.7 (b) shows the height distribution of the islands and the rest of the sample. Fig. 3.8 shows a 3-D image of the same region. Outside the region of the electric field, the gold surface remains mostly planar, like it was before the experiment, except for some thermal roughening. The islands get initiated along the edge and the density of these islands decreases towards the center of the electrode, where the electric field is uniform. Fig. 3.9 (a) shows a closer view of these islands from the same experiment. Also Fig. 3.9 (b) is the line scan across a cross section showing the height distribution of these islands. Fig. 3.9 (c) shows a 3-D view of the same region. The in-plane island dimension of 1-2 μm is several times the average grain size (30 – 100 nm) of the gold film. The height of the islands in the two bands varies from 50-150 μm. Note that the vertical magnification in Fig. 3.9 (c) and Fig. 3.8 is much higher than the in-plane magnification, which causes the islands to appear like pillars, although they are more like shallow domes.

In another experiment with an electrode of width 50 μm, carried out at similar conditions, a comparable result is observed, with lower density of islands, as shown in Fig. 3.10. It could be reasonably concluded that lower island density of Fig. 3.10 represents an earlier state of island evolution shown in Fig. 3.7.

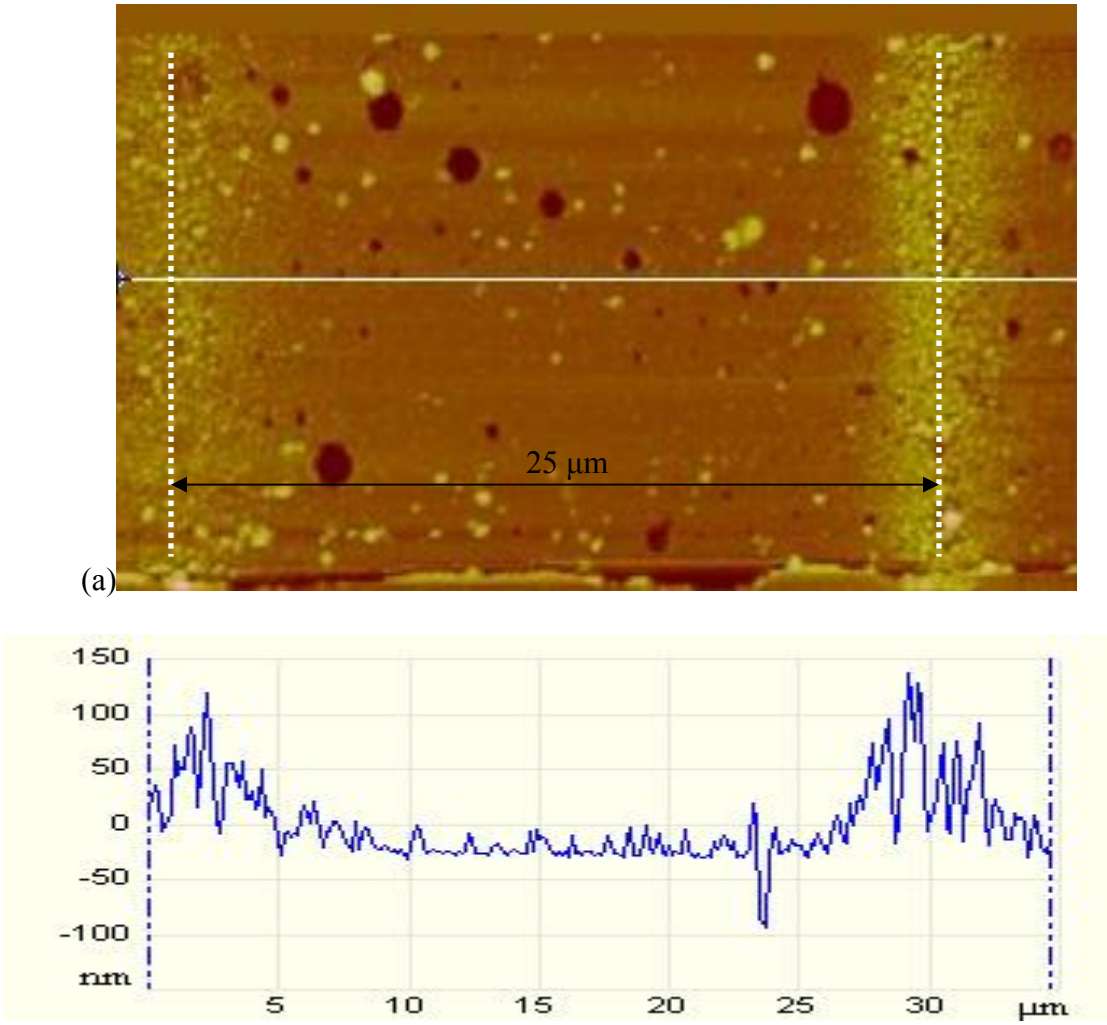

Figure 3.7: Representative experimental results. The dashed line is the approximate location of the edge of the top titanium electrode. (a) Top view of the gold sample showing island population distribution under both edges. The titanium electrode runs between the two dashed lines. $T = 280^{o}C$, $t = 4.5$ hr, $E = 5x10^{8}$ V/m. (b) Line scan showing the height distribution of the sample along the solid line.

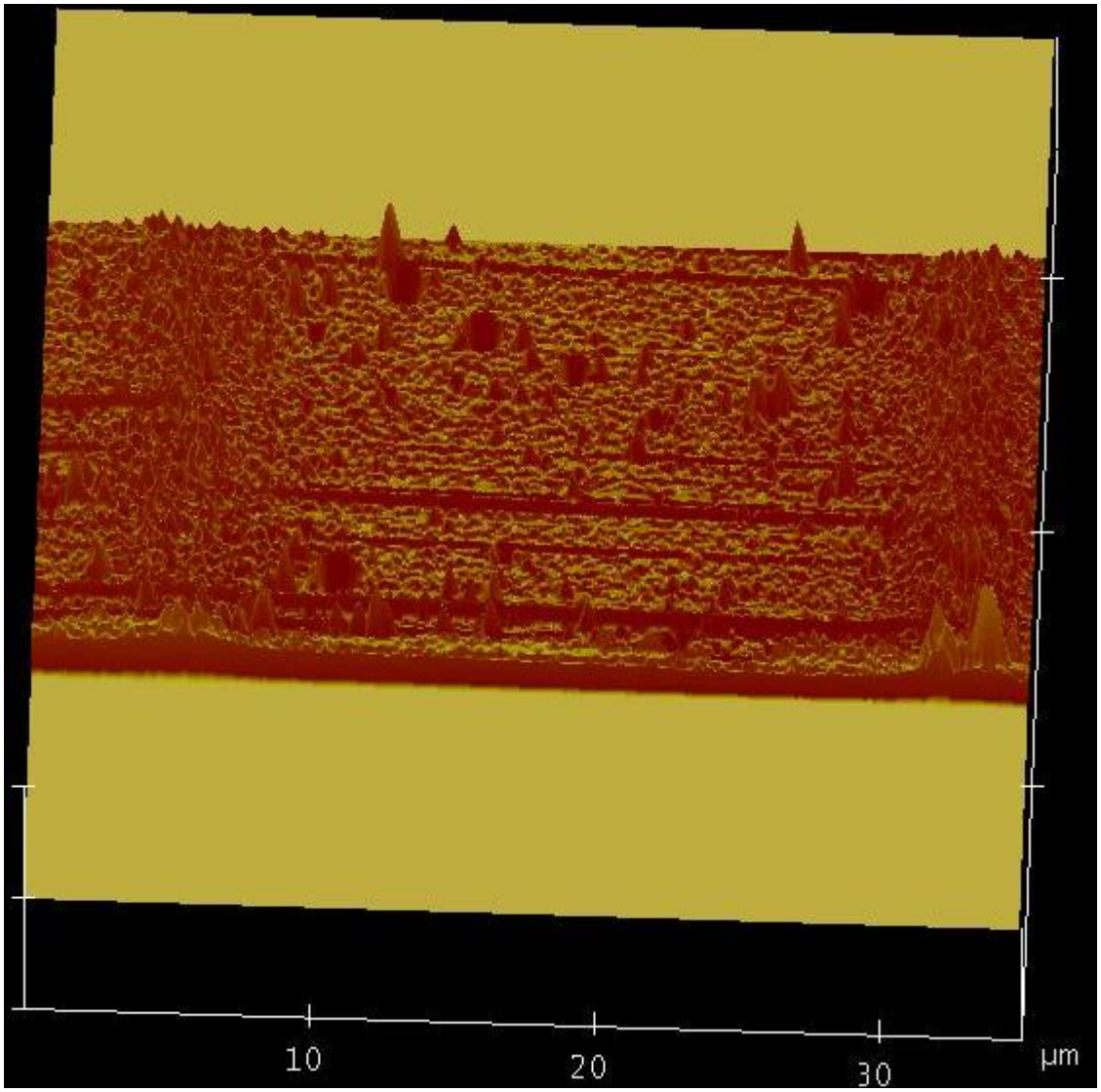

Figure 3.8: 3-D image showing growth of islands under the edge of a 25 µm wide electrode for an experiment carried out at T = 280^{o}C, t = 4.5 hr, E = 5x10^{8} V/m.

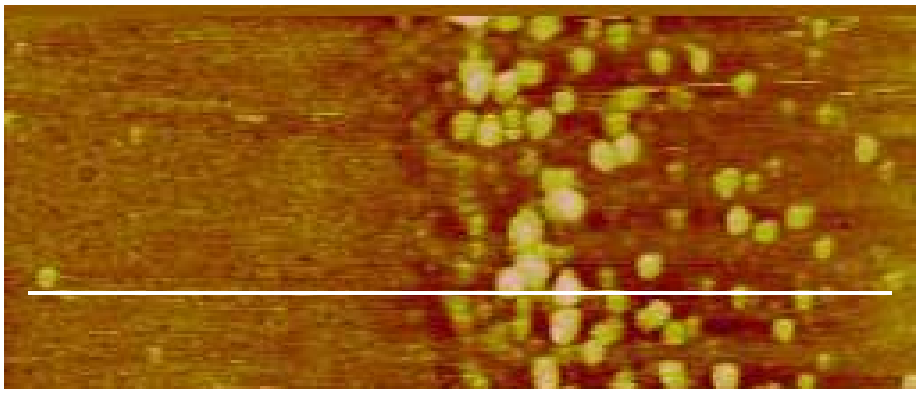

(a)

(b)

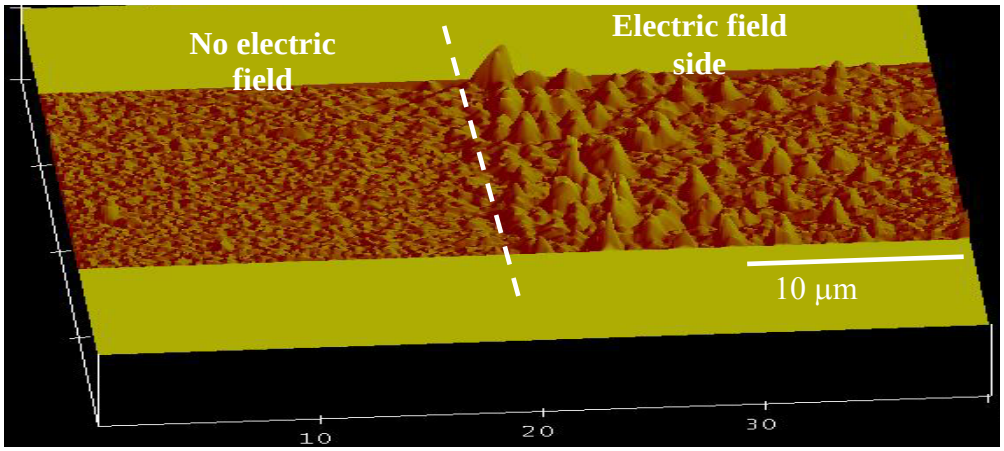

(c)

Figure: 3.9 (a) Island growth under the edge of the electrode. (b) A line scan of the islands showing the island height distribution. (c) 3-D view of the island growth.

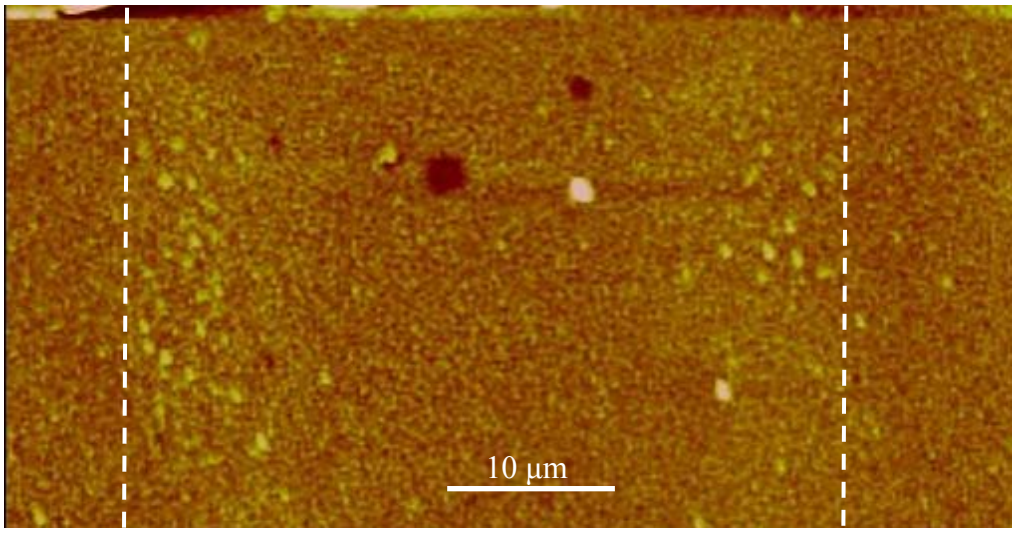

Figure 3.10: Top view of the gold sample showing island population distribution under both edges. The titanium electrode runs between the two dashed lines. T = 280 ^{o}C, t = 4.5 hr.

An earlier stage of the island growth process was captured in another experiment of 7 hr duration at 350^{o}C, which is shown in Fig. 3.11, where the islands are mostly confined to the electrode edge. Note that the temperature and the time are higher in this experiment to form an island chain than those in the experiments described earlier in which the island density was greater. The discrepancy indicates variability in the magnitude of the applied electric field, which is not precisely controllable due to long wavelength waviness of the glass plates. However, the main conclusion from these experiments is that, under well regulated experimental conditions, density and location of island population can be controlled by the fringe field position.

Thermal pitting and roughening due to grain boundary grooving was observed uniformly everywhere on the gold surface in higher temperature experiments of around 300 ^{o}C.

Within the uniform field region, near the center of the electrode, some of the experiments showed growth of sparsely populated features as seen in Fig. 3.7. However, by comparison with the areas that did not experience any electric field, they were concluded to be due to thermal roughening, rather than the instability induced by the uniform electric field described in chapter 2.

Thus, the experiments reported here with wide electrodes are, to the best of the author's knowledge, the first controlled demonstration of the phenomenon of electric field induced surface diffusion on metals and the ability to grow island populations within the fringe field, driven by the gradient in the electric field.

It is worth noting from Fig. 3.7 that the islands that form along the electrode edge form a band, the width of which is 5 – 10 μm. However, from Fig. 2.7 in previous chapter, a strong gradient in electric field is confined to a width of about $5d \sim 1\ \mu m$. Clearly, the growth of islands extends beyond the area of strong gradient, although at a decreasing density, into the area of uniform field. This observation points to a coupling between the two island growth mechanisms discussed earlier, i.e. instability in uniform field and growth driven by field gradient, which can be qualitatively described as follows. The rate of growth of instability in the interior is initially low because the amplitude of the initial perturbation (or, roughness) is small. However, as the islands grow near the edge driven by the field gradient there, they provide higher perturbation amplitude for the instability to grow in the adjacent uniform field region. Thus, growth of islands is expected to proceed progressively from the edge towards the interior, with decreasing density and amplitude, consistent with the experimental observations. This idea can be made quantitative by considering a 3-D perturbation analysis in which the field is

uniform in one direction and has a gradient in the perpendicular direction. Further discussion is deferred to a later section.

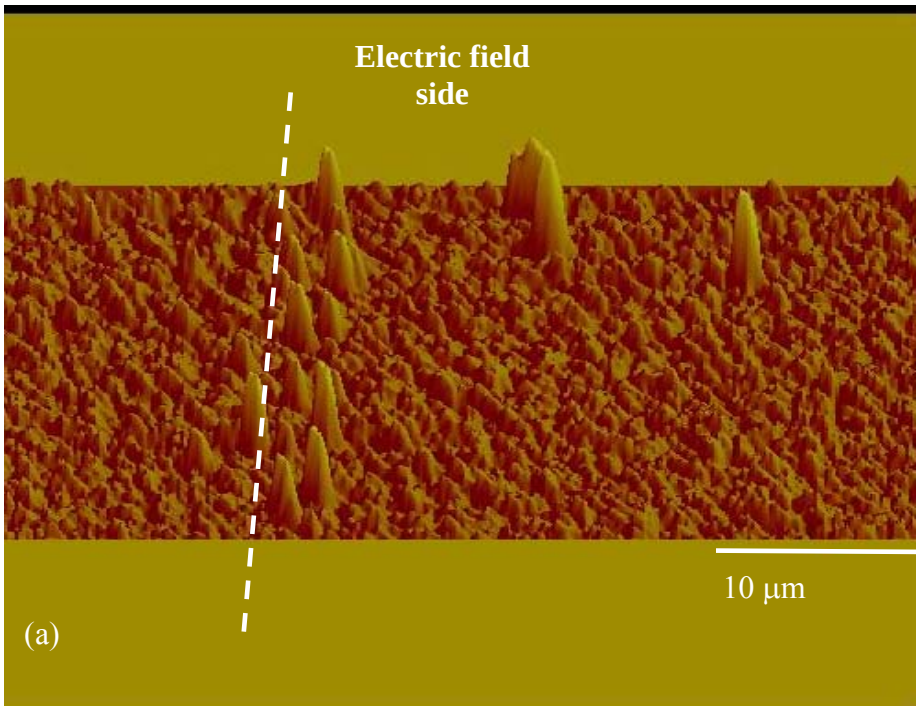

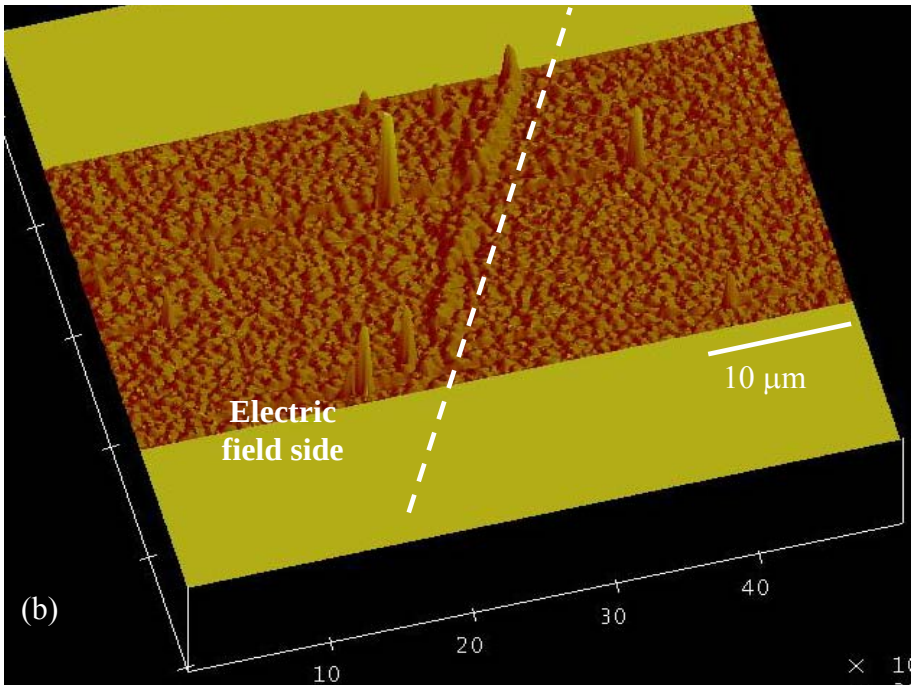

Figure3.11: Representative experimental results for the case of a wide electrode for the early stage of island growth, confined mainly to a row along the electrode edge. The dashed line is the approximate location of the edge of the top titanium electrode. T = 350 ^{o}C, t = 7 hr. The maximum island height is about 70 nm.

3.4.2 Medium electrode size (~10 μm)

Although the wide electrodes demonstrate the ability to grow sub-micron scale islands near the electrode edges, it is necessary to demonstrate growth of individual surface features in order to realize patterned growth. Moving in that direction, the electrode width was reduced to less than 10 μm in the next set of experiments. The choice of the electrode width was guided by the width of the island band observed in Fig. 3.7, which is approximately 7-8 μm. The objective is to observe if the island bands begin to interact and merge, without the region of little activity in the middle.

Titanium electrodes of 7 μm width were used, and the experiments were carried out at 280 ^{o}C for 4 *hrs* with an applied electric field of about $5x10^{8}$ *V/m*. Once again, as in previous experiments with large electrode sizes, growth of islands along two bands under the two edges of the electrode was observed. However, these bands are no longer distinctly separated and they are seen to begin to merge in the center and form a single wide band of islands. One of the results can be seen in Fig. 3.12 (a), with a line scan showing island height distribution in Fig. 3.12 (b). Also a 3-D image can be seen in Fig. 3.13. Results from a similar experiment carried out with a titanium electrode of 4.5 μm width at 250 ^{o}C for 3hours with an applied electric field of approximately $5x10^{8}$ *V/m* is shown in Fig. 3.14 and 3.15. Once again the two bands appear to merge at the center, consistent with the expectations based on the wider electrode experiments. Note that some of the island formation is due to thermal roughening; it has proven to be a challenge to completely de-couple thermal roughening from the electric field induced diffusion.

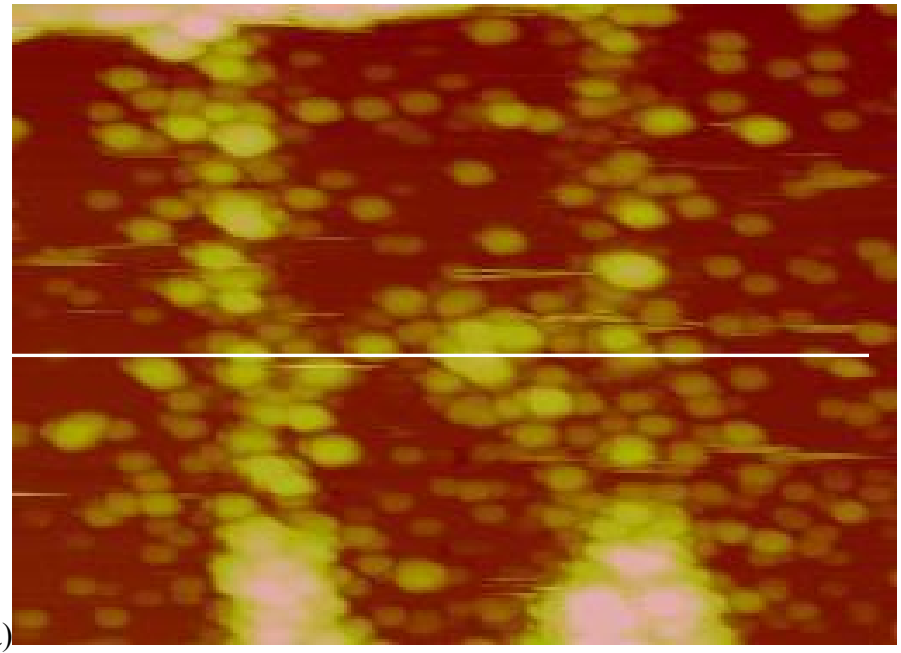

(a)

(b)

Figure 3.12: (a) Top view of the gold surface as a result of an experiment with electrode width of 7 µm, carried out at 280 ^{o}C for 4 hours with an applied electric field of 5x10^{8} V/m. (b) Line scan along the solid line showing the island height distribution.

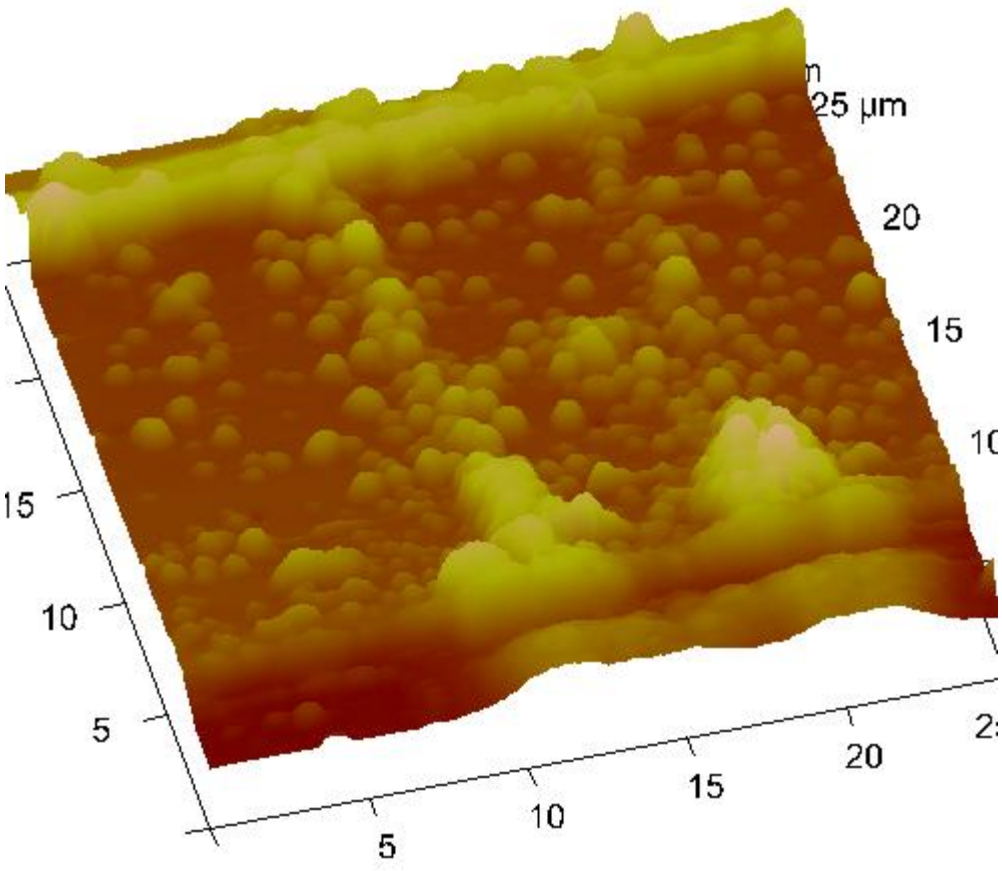

Figure 3.13: 3-D image of the gold surface as a result of an experiment with electrode width of 7 µm, carried out at 280 ^{o}C for 4 hours with an applied electric field of 5x10^{8} V/m.

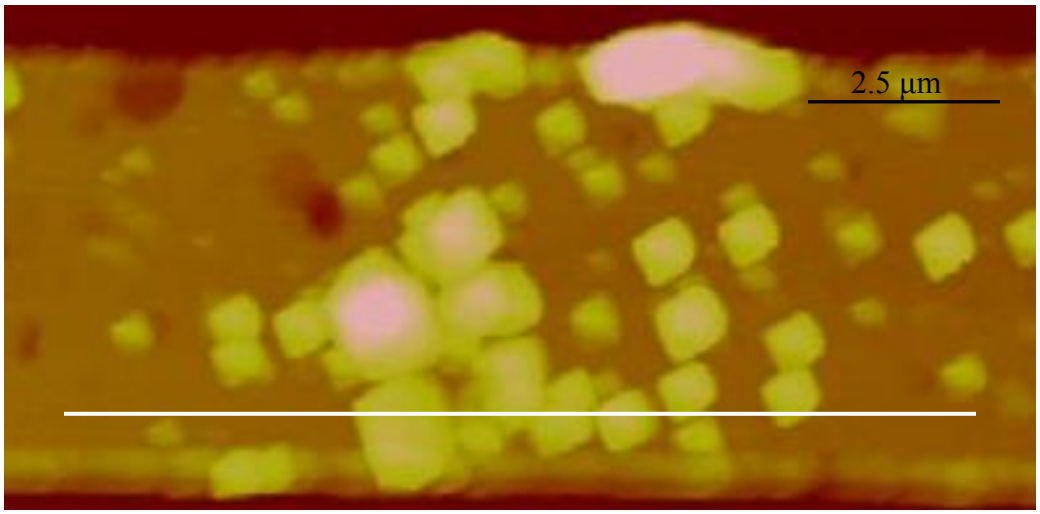

(a)

(b)

Figure 3.14: (a) Top view of the gold surface as a result of an experiment with electrode width of 4.5 µm, carried out at 250 ^{o}C for 3 hours with an applied electric field of 5x10^{8} V/m. (b) Line scan along the solid line showing the island height distribution.

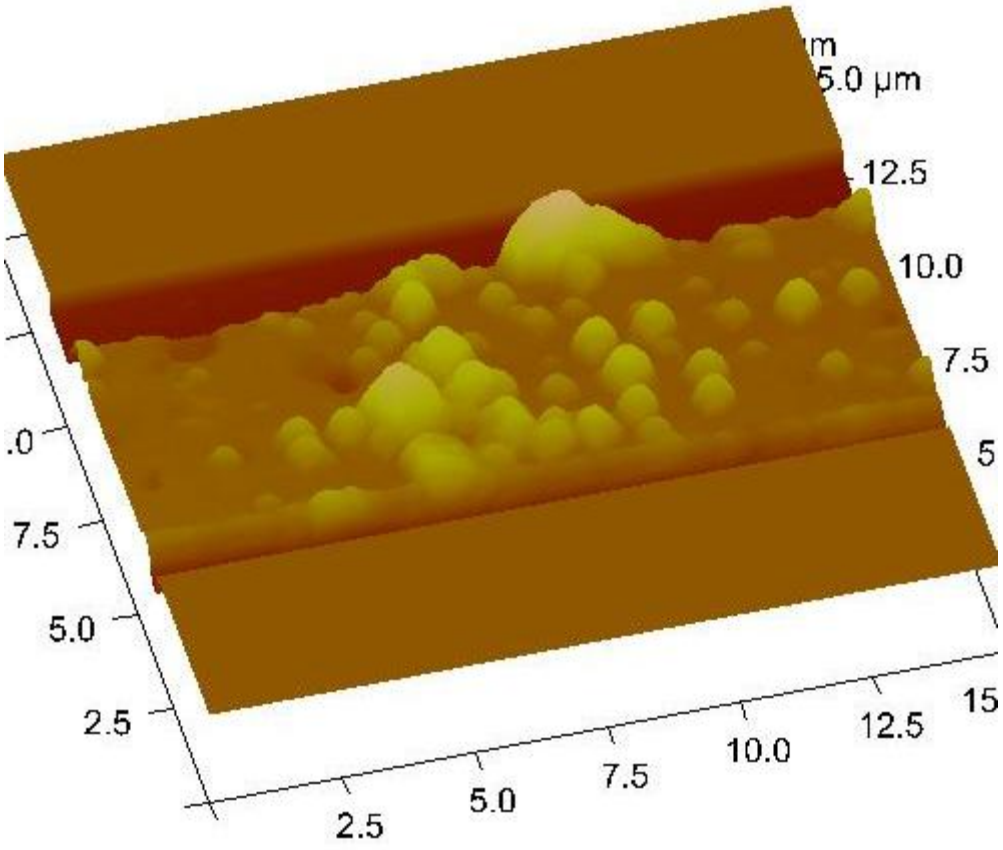

Figure 3.15: 3-D image of the gold surface as a result of an experiment with electrode width of 4.5 µm, carried out at 250 ^{o}C for 3 hours with an applied electric field of 5x10^{8} V/m.

3.4.3 Small electrode size (< 5 µm)

As seen in previous sub-section, for an electrode width of 5-7 *µm*, the two separate bands begin to coalesce at the center, but do not completely form a single band. The next set of experiments was carried out with top electrode size smaller than 5 *µm*.

Figs. 3.16 and 3.17 show the results of using an electrode with a width of 1.3 *µm*, (280 ^{o}C for 4 hours with an applied electric field of 5x10^{8} *V/m*), which shows formation of a continuous ridge under the electrodes, flanked by valleys on either side. Thus, at 1

μm electrode dimension, there is a transition from band of islands to a single ridge. Such a transition is not completely unexpected because the average in-plane dimension of the islands in the wider electrode experiments was about 1 μm. Thus, these experiments demonstrate that micron scale features can be grown controllably by means of electric fields. Note that, similar to most other experiments in this study, the samples undergo thermal roughening due to polycrystallinity of the samples. In order to isolate electric field induced island growth from thermal roughening, it would be desirable to use single crystal samples, which is beyond the scope of the current work. Fig. 3.17(a) shows a close up view of the ridge and the height profile can be seen along the solid line in Fig. 3.17(b).

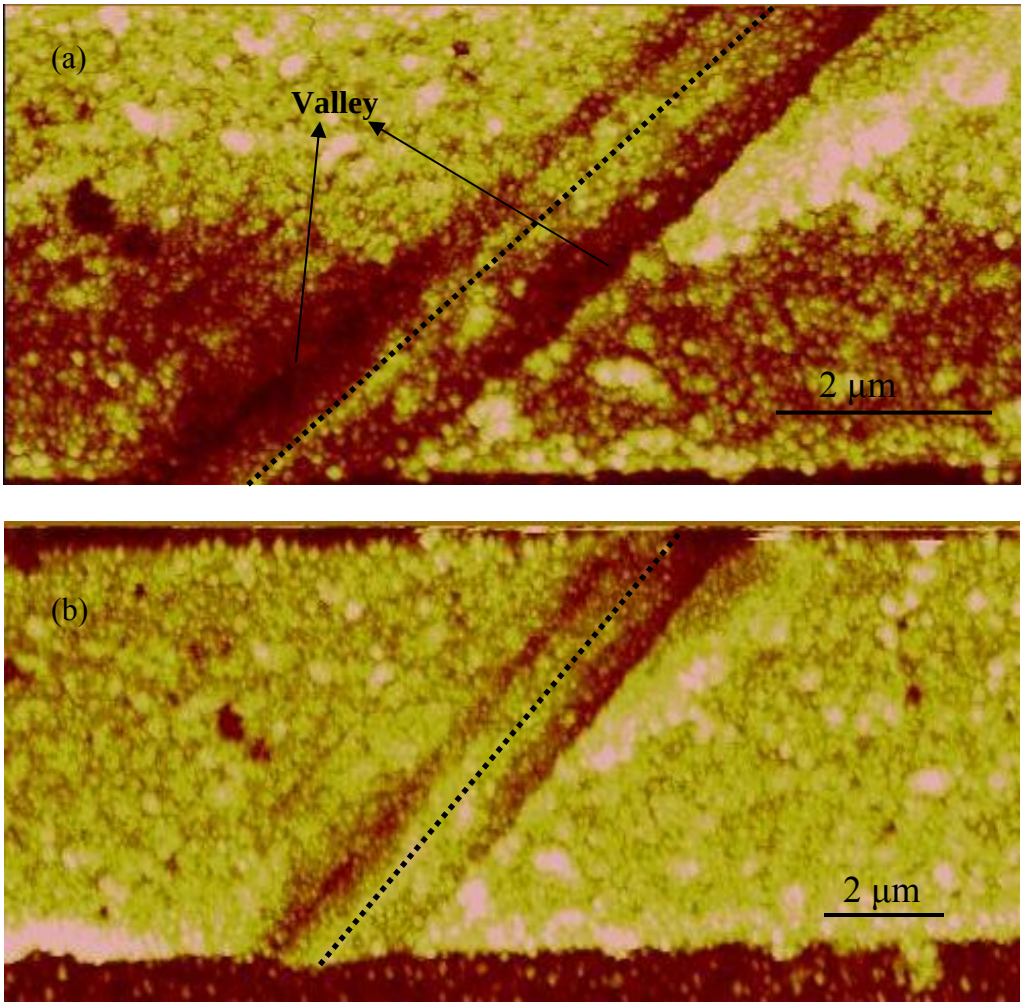

Figure 3.16: (a), (b) Top view of the gold surface as a result of an experiment with electrode width of 1.5 μm, carried out at 280 ^{o}C for 4 hours with an applied electric field of 5x10^{8} V/m with the dashed line showing the electrode position. The two images are from two different spots on same electrode.

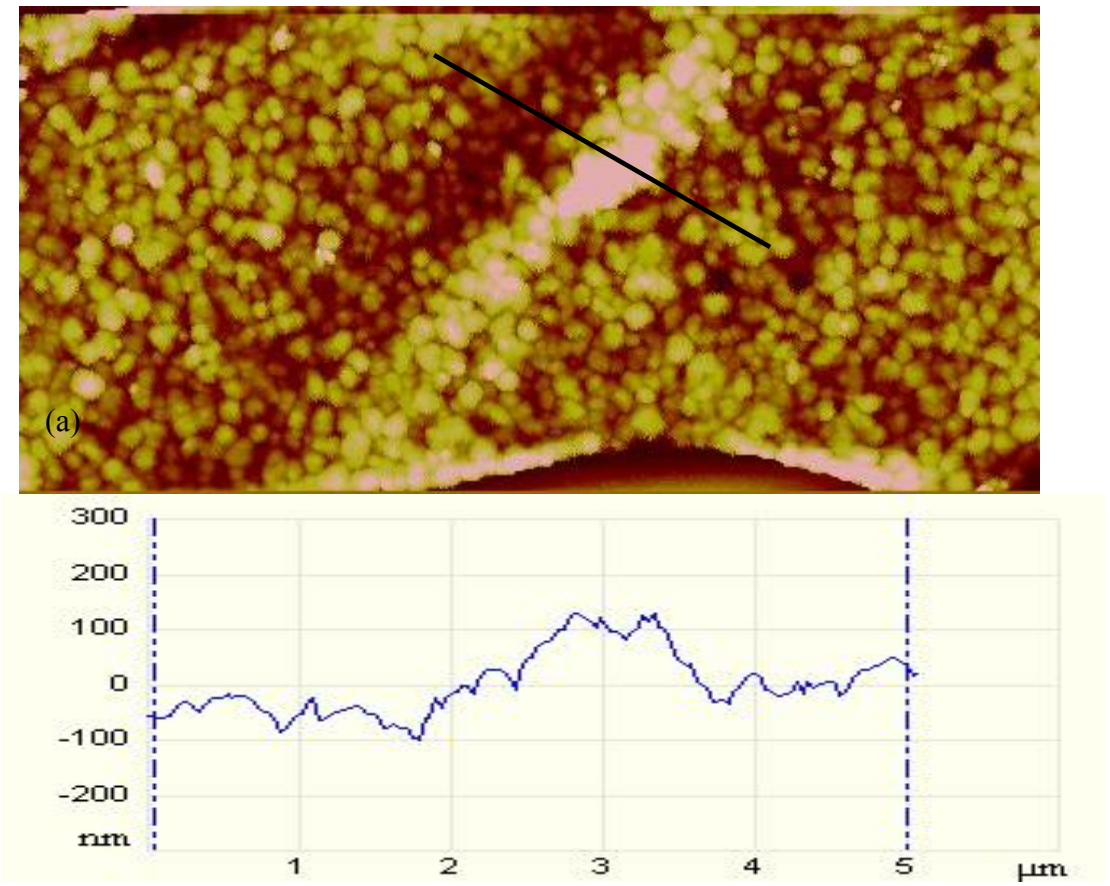

(b)

Figure 3.17: (a) Top view of the gold surface as a result of an experiment with electrode width of 1.5 µm, carried out at 280 ^{o}C for 4 hours with an applied electric field of 5x10^{8} V/m with the dashed line showing the electrode position (b) The height profile of the surface along the solid line.

3.5 Summary

- The experimental investigation demonstrates that electric field can cause significant surface diffusion and island formation on gold at temperatures of around 250 – 300 ^{o}C.
- Most of the activity is primarily confined to the electrode edges, where the gradient in the electric field provides a strong driving force for surface mobility. The analyses of the preceding chapter suggest that surface evolution and island

formation in the present experimental geometry can occur through two mechanisms: (i) surface evolution in the gradient field near the edges and (ii) surface instability in the uniform field region in the interior of the capacitor. It appears that, for the present experimental configuration and parameters, the former mechanism operates more readily than the latter. This can be rationalized by examining the characteristic growth times in each case. As already shown in the preceding sections, for $T = 250\ ^{o}C$, $\delta = 0.5\ nm$, $\Omega = (0.5\ nm)^3$, $T_M = 1338$ K, $d = 0.2\ \mu m$, and $E = 5 \text{ X } 10^8\ V/m$, the characteristic time for the growth of islands in the uniform field region (defined as the time for growth of islands to approximately 1.6 times the initial amplitude) is about 8000 *s*. At the same parameters, the characteristic time for growth of islands at the edge of the capacitor (defined as the time for growth of the islands to the gap height) is about 4400 *s*. Note the difference in the definition of characteristic time in each case. Thus, it would take roughly $4 \text{ x } 10^3$ *s* for the edge islands to grow to a height of 200 *nm*; whereas, starting from an initial roughness of 6 *nm*, it would take approximately $6 \text{ x } 10^4$ *s* for the interior surface instabilities to grow to a comparable height. The time for the interior instability to result in observable features appears to be much longer than that for the appearance of the edge features; as a result, the latter phenomenon is expected to dominate the experimental observations. Thus, it is not surprising that observed islands were predominantly located near the electrode edges.

- In order to investigate the effect of electrode width on island growth, progressively thinner titanium electrodes were employed. When the width is

comparable to the width of the band of islands observed in Fig. 3.7, the two distinct islands near the edges appear to merge and form a single band of islands.

- However, in order to grow a single island on a surface, it is necessary to use an electrode whose width is comparable to the average dimension of a single island. For the case of 1.3 μm electrode width, the islands were replaced by a single continuous ridge. Thus, under well controlled experimental conditions, it should be possible to grown individual micron sized islands in any desired pattern.
- It is worth noting that, since the gold film is polycrystalline, thermal roughening appears to compete with surface diffusion due to electric field. However, in order to obtain cleaner surface quality, it is recommended that single crystal samples be used in future experiments.

Chapter 4

Numerical Modeling

4.1 Introduction

An analysis of electric field induced surface diffusion was presented in chapter 2, based on energetic and kinetic considerations, which proved to be a good starting point in explaining the experimental results discussed in chapter 3. Particularly, calculation of the driving force for diffusion in the fringe field provides a good explanation for island growth along the edges of the electrode. The normal velocity profile based on the Maxwell-Rogowski fringe field solution is expected to be a good approximation for surface evolution when electric field is just turned on. However, as the surface deviates from the flat configuration, the electric field also evolves and the surface curvature begins to contribute to the chemical potential. As a result, surface normal velocity evolves in time and is no longer given by the analyses in chapter 2. It is necessary to carry out numerical analysis to track surface evolution beyond small perturbations and to determine the growth rates and eventual equilibrium island shapes.

Also, as observed in the experimental results, the surfaces evolve differently as the electrode width is decreased while keeping the distance between the electrodes constant. For a large electrode size (~ 20 μm), two separate bands of islands, one at each edge of the electrode, are observed. As the electrode size is decreased (~ 7 μm), the two separate bands tend to merge. For even smaller electrode size (~ 1μm), only one, almost continuous ridge is observed under the electrode. Even though the analytical treatment

provides some insights into these observations, it is far from satisfactory. The analytical analysis does not describe how the surface evolution changes from two separate bands to a single ridge as the electrode width is decreased. To answer these questions and gain further insight, finite element analysis has been carried out.

4.2 Model Formulation:

The numerical formulation consists of two parts. One part involves solving for the electric field between the two electrodes. In the second part, the electric field from the first step is used to calculate the surface chemical potential, which is then used to calculate surface normal velocity. Surface evolution due to diffusion and the modified electric field, which are coupled to each other, are computed and updated in each time step.

4.2.1 Surface Diffusion

As discussed in chapter 2, the governing equations for surface diffusion over the test surface can be summarized as follows. Chemical potential per surface atom is given by:

$$\mu = \Omega(U_e - U_E - \kappa\gamma) \tag{4.1}$$

where Ω is the atomic volume, U_e is the elastic energy density, U_E is the electrostatic energy density, κ is the local curvature of the surface and γ is the surface energy per unit area. The mass flux on the surface due to this chemical potential is given by:

$$j = \frac{-D_s C_s}{kT} \nabla_s \mu \tag{4.2}$$

Where D_s is the surface diffusivity, C_s is the concentration of diffusing atoms, k is the Boltzman constant, T is the absolute temperature and ∇_s is the gradient operator along the surface and s is the arc length along the test surface. By mass conservation, the surface normal velocity can be expressed as:

$$V_n = \frac{D_s C_s \Omega^2}{kT} \nabla_s^2 \mu = \frac{D_s C_s \Omega^2}{kT} \nabla_s^2 (-U_E - \kappa\gamma) = \frac{D_s C_s \Omega^2}{kT} (-U_{E,ss} - \kappa_{,ss}\gamma) \tag{4.3}$$

The Elastic energy density U_e is neglected in the problem. For a nearly flat surface where the x-axis is aligned along the surface and the y-axis is normal to the surface, s can be approximated as x. In that case the above equation can be approximated as:

$$\frac{dy}{dt} = \frac{D_s C_s \Omega^2}{kT} (-U_{E,xx} - \kappa_{,xx}\gamma) = \frac{D_s C_s \Omega^2}{kT} (-\frac{1}{2}\varepsilon_o (E^2)_{,xx} - \gamma y_{,xxxx}) \tag{4.4}$$

Where

$$U_E = \frac{1}{2}\varepsilon_o E^2 \tag{4.5}$$

and

$$\kappa = y_{,xx} \tag{4.6}$$

ε_o being the permittivity of vacuum and E is the applied electric field. The experimental geometry can be approximated by Fig. 4.1. As seen in Fig. 4.1, d is the distance between the electrode and the surface, w is the width of the electrode, V^* is the voltage difference between the two electrodes and the all surface segments are marked by numbers 1 through 8. Surface 1 is the only evolving one. The parameters appearing in Eq. 4.4 can be normalized as following:

$$x' = x / d,\ y' = y / d,\ E' = E / E_o,\ E_o = V^*/d,\ t' = t / \tau \tag{4.7}$$

In terms of the above non-dimensional variables, Eq. 4.4 can be re-written as

$$\frac{dy'}{dt'} = \frac{1}{2}\varepsilon_o E_o^2 \frac{d}{\gamma}(E'^2)_{,x'x'} - y'_{,x'x'x'x'} \tag{4.8}$$

where

$$\tau = \frac{kTd^4}{D_s C_s \Omega^2 \gamma} \tag{4.9}$$

Eq. 4.8 can be re-written as:

$$\frac{dy'}{dt'} = \alpha (E')^2_{,x'x'} - y'_{,x'x'x'x'} \tag{4.10}$$

where

$$E' = \frac{E}{E_o} = \frac{Ed}{V^*} \tag{4.11}$$

$$\alpha = \frac{qV^{*2}}{\gamma d},\ q = \frac{\varepsilon_o}{2} \tag{4.12}$$

α represents the driving force for the surface to roughen due to the electric field.

The surface evolution equation Eq. 4.8 is subject to the following boundary conditions

- Zero mass flux (j=0 in Eq. 4.2) at points A and B because they are very far away from the electric field region and no mass is transferred from outside or from inside to outside through these points.
- Zero slope for surface 1 at point A. This condition ensures that surfaces 1 and 8 remain perpendicular to each other at all times.

- Zero slope for surface 1 at point B. This condition ensures that surfaces 1 and 2 remain perpendicular to each other at all times.

The initial condition for Eq. 4.8 is $y = 0$. The electric field between the electrode and the surface changes as the surface evolves in time. The externally applied potential V^* is kept constant.

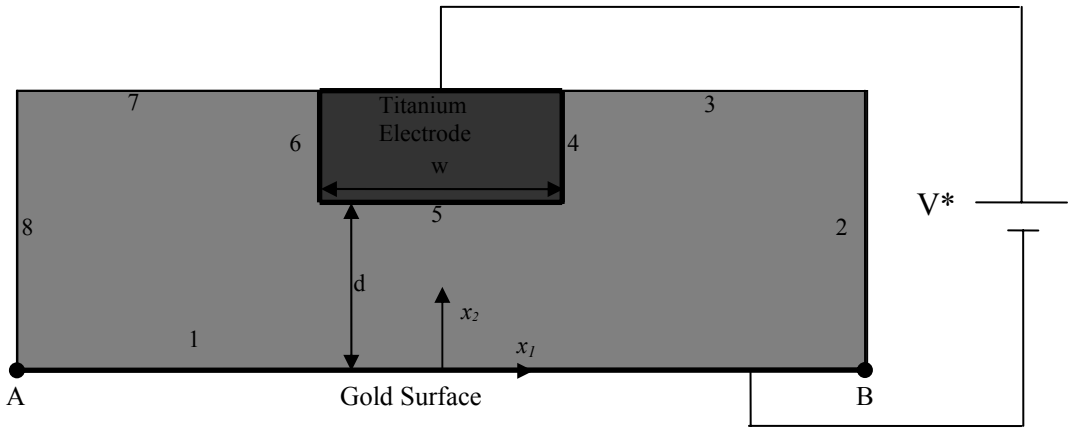

Figure 4.1:Schematic of the experimental setup being analyzed using FEM, where Laplace equation $V_{,ii}=0$ is solved in the lightly shaded region enclosed by surfaces 1 through 8. Surface1 is the conductive surface on which the diffusion equation is solved. Surfaces 4, 5, 6 represent the electrode which is at a potential V higher than the surface 1. Surfaces 2,3,7,8 are no flux boundaries and far away from the fringe electric field.*

4.2.2 Electrostatic Field

Re-naming (x,y) with (x_1,x_2), the potential at any point (x_1, x_2) in the lightly shaded region in Fig. 4.1 can be denoted by $V(x_i)$. From the Maxwell's equations,

$$V_{,ii} = 0 \tag{4.13}$$

One can evaluate the electric field throughout the lightly shaded region in Fig 4.1 by solving Eq. 4.13. A voltage V^* is prescribed on surfaces 4, 5 and 6, which represent the titanium electrode and zero on surface 1, which represents the gold surface. Additionally $\frac{\partial V}{\partial n} = 0$ on the remaining surfaces (surfaces 2, 3, 7, 8 in Fig 4.1), where n is the outward surface normal, assuming that they represent charge free surfaces.

4.3 Numerical Procedure

Finite element method is used to solve the field equations outlined in the previous section (Eq. 4.8, Eq. 4.13). Given the potential difference and geometry of electrode surfaces at time t, the problem is to compute the surface normal velocity distribution and the change in the surface during a time interval Δt. Full details of the numerical procedure can be found in Xia *et al* (1997). The author acknowledges Prof. A.F. Bower (Division of Engineering, Brown University, Providence, RI) for providing the FE code used in these computations. The first step is to calculate the potential distribution $V(x_i)$ in the region between two surfaces at time t by solving the Laplace equation Eq. 4.13. In order to use the finite element method, Eq. (4.13) can be re-written in weak form as

$$\int_R V_{,i}\,\delta V_{,i}\,dA = 0 \qquad (4.14)$$

where R is the 2D region between the titanium and gold surfaces and δV is an admissible variation in voltage with $\delta V = 0$ on surfaces with prescribed voltage. A typical finite element mesh consisting of three-noded triangular elements is shown in Fig. 4.2. The region is continuously remeshed using an advanced front algorithm as it changes its shape. Solution to the electrostatic problem enables calculation of the electric field at the

gold surface and thus its contribution to the surface chemical potential. The surface diffusion equation is then solved to determine the surface velocity and shape change during a time interval Δt. Rewrite Eq. (4.3) in its weak form as

$$\int_{\Gamma} V_n \delta V_n ds = \frac{D_s C_s \Omega^2}{kT} \int_{\Gamma} \left(U_{E,s} + \gamma \kappa_{,s} \right) \frac{\partial \delta V_n}{\partial s} ds \tag{4.15}$$

The gold surface is discretized using a one-dimensional mesh and Eq. (4.14) is solved for the surface normal velocity V_n, using the finite element method. Eq. (4.14) and (4.15) is integrated with respect to time using a semi-implicit Euler time stepping scheme.

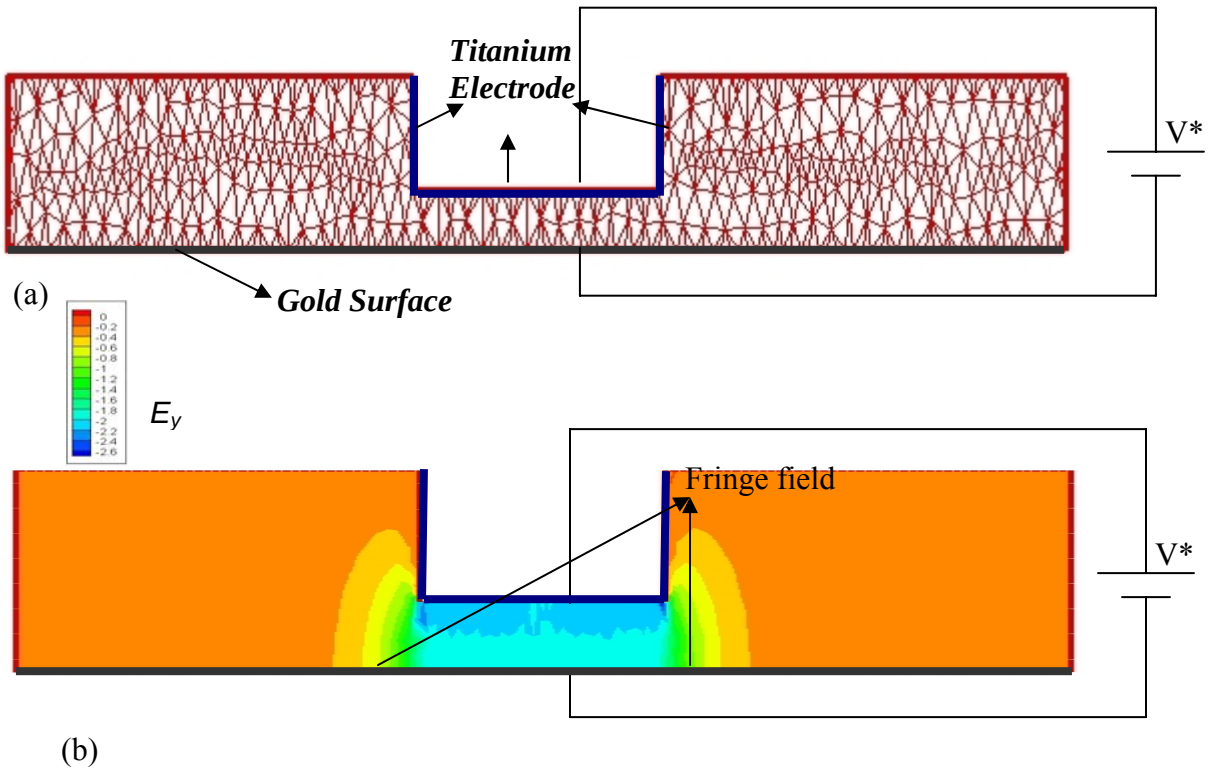

Figure 4.2: Initial Geometry at t=0 (a) Initial Mesh, (b) Contours of y-component of Electric field at t=0, showing fringe field at the edges of the electrode.

4.4 Results

It was shown in chapter 2 that a conducting surface subjected to a uniform electric field is unstable with respect to perturbations above a critical wavelength. In order to examine such instability, a FEM study was carried out for the case of a parallel plate capacitor with an initially flat surface, in which the lower plate has a significantly higher diffusivity than the upper plate. For the simulations the upper plate is given zero diffusivity. The overall length of the plates is 20 times larger than the distance d between them. This large length ensures absence of edge effects in the central region and simulates the large electrode case discussed in the preceding chapter. The upper plate is held at a potential V^* higher than the lower plate. For a real physical system, if $d = 200$

nm and $V^* = 200\ V$, then $\alpha = -1$, where $\gamma=1$ and $q=-1$, in the simulation represents an electric field of $10^9\ V/m$ in the real physical system. The results show that the flat surface is indeed unstable when subjected to a uniform normal electric field; the numerical simulation captures the kinetics into large shape change regime. The results of this analysis can be seen in Fig 4.3

The wavelength of the fastest growing perturbation for this analysis is *10.0*. The analytical value of the fastest growing perturbation for this case can be calculated using Eq. 2.34 from Section 2.4 and it comes out to *8.9*. The simulation and analytical results are quite close to each other in predicting the fastest growing wavelength.

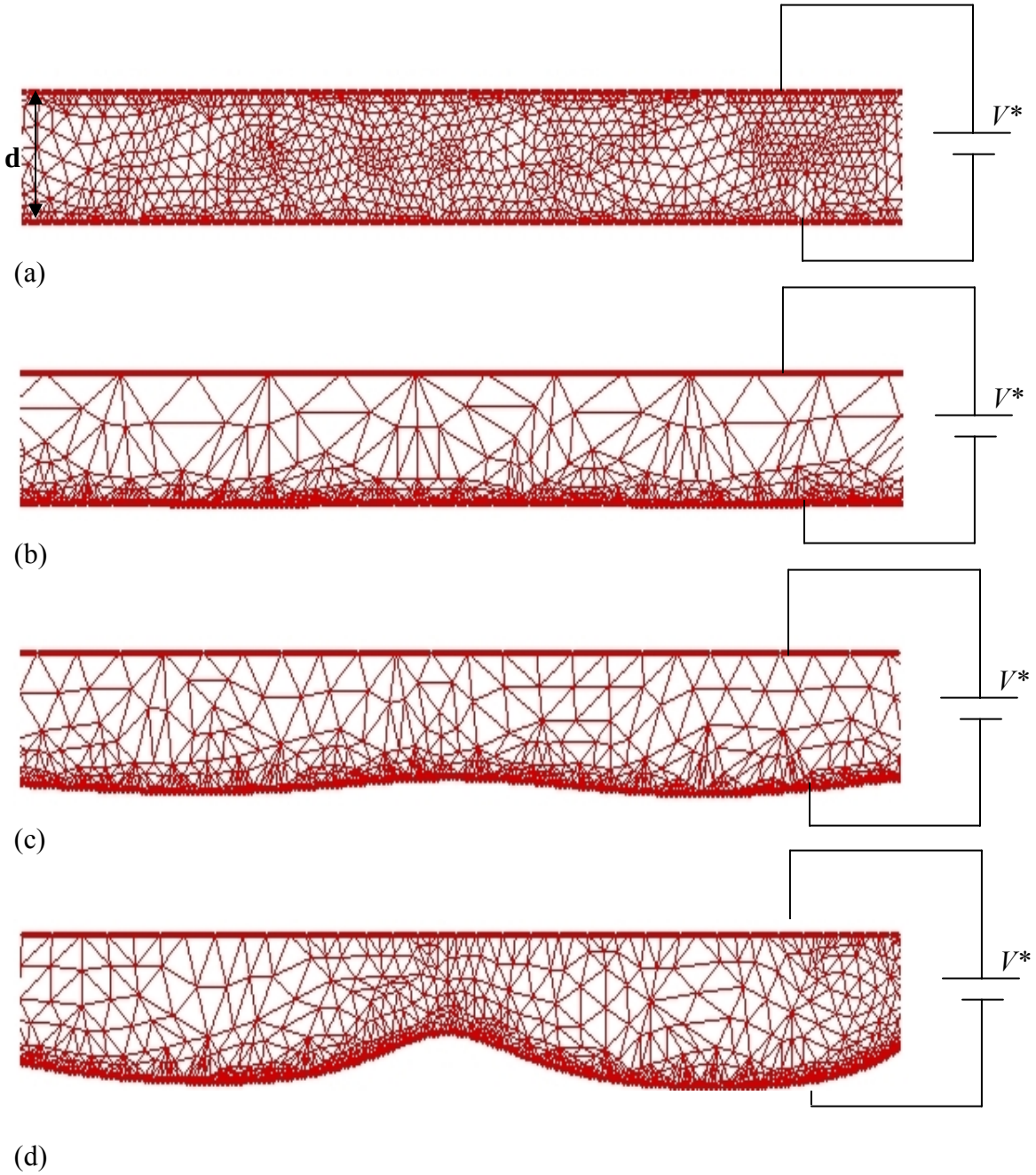

Figure 4.3: A parallel plate capacitor configuration where bottom plate has relatively high diffusivity and is held at a potential V lower than the upper plate and where* $\alpha = -1$, where $\gamma=1$ and $q=-1$ *,(a) at* $t/\tau=0$, *(b) at* $t/\tau = 139$, *(c) at* $t/\tau = 155$, *(d) at* $t/\tau = 162.5$.

Fig. 4.4 shows the $Abs(\alpha)$ versus t/τ, where $\gamma = 1$, $q = -1$, for the instability amplitude to grow to 25% of initial distance, d, between the plates. As can be seen the time required for the perturbation is a strong function of α, which is a function of applied electric field across the plates. The time required increases quite sharply as the applied electric field is reduced. From Eq. 2.35 in Chapter 2, it was shown that the time required for the perturbation to grow is proportional to $1/E^4$, where E is the applied electric field. It can be seen from the straight line in Fig. 4.5 that the normalized time for the perturbation to grow is directly proportional to $1/\alpha^2$, where $\gamma = 1$, $q = -1$.

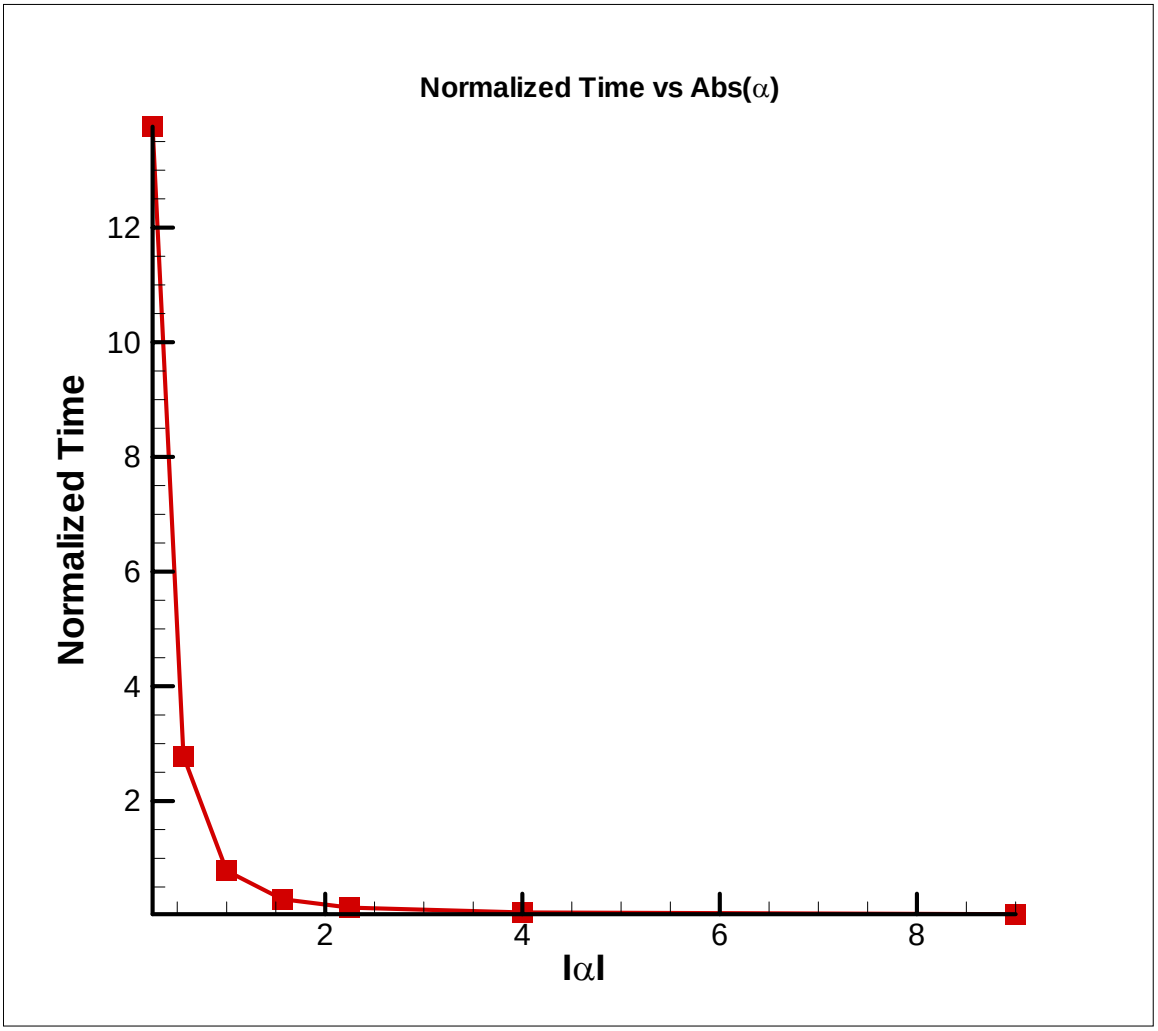

Figure 4.4: Abs(α) vs Normalized time (t / τ) for the amplitude of the instability to grow to 0.25d for an initially flat surface in parallel plate capacitor.

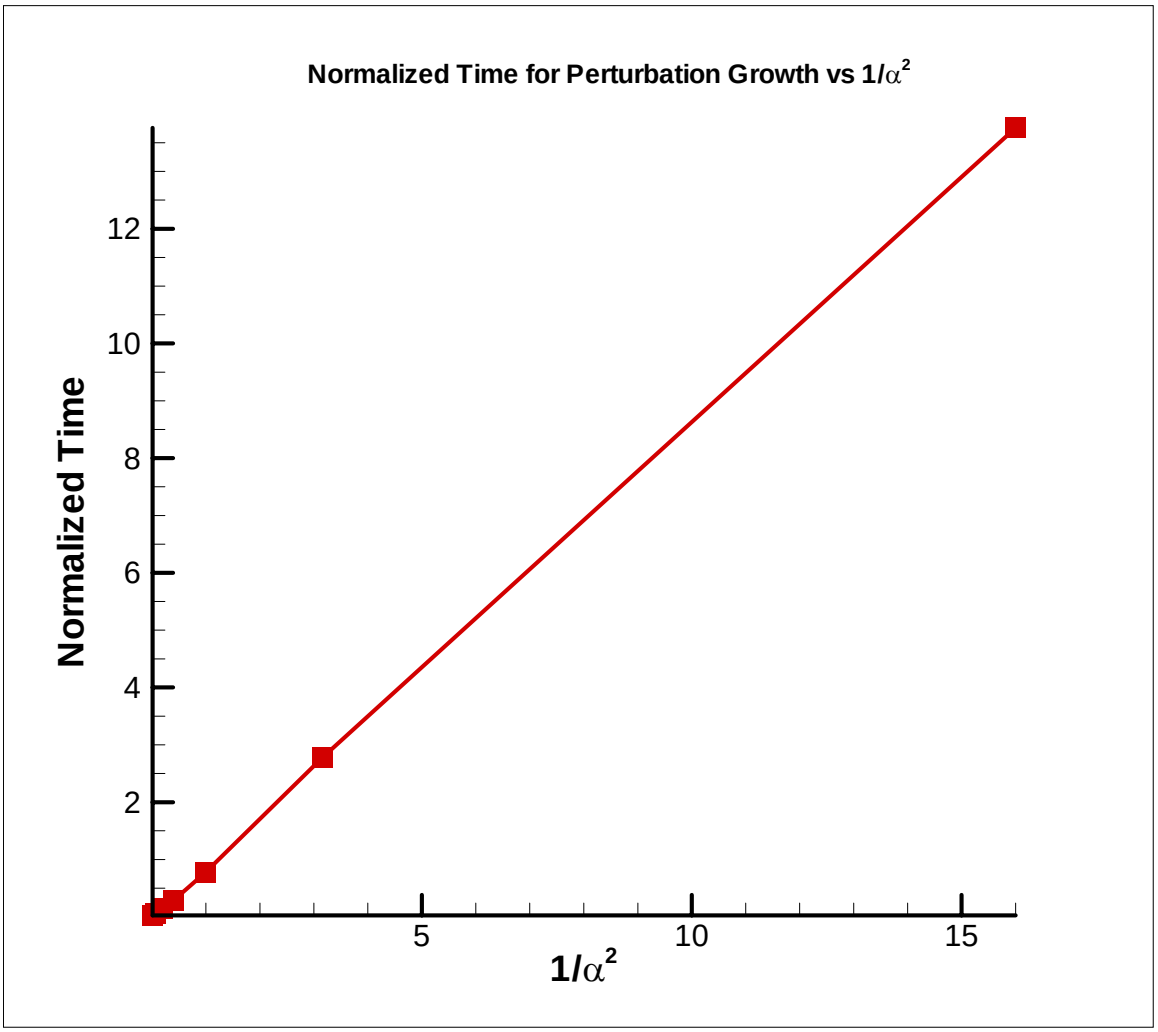

Figure 4.5: $1/\alpha^2$ vs Normalized time (t / τ) for the amplitude of the instability to grow to 0.25d for an initially flat surface in parallel plate capacitor.

Fig. 4.6 shows how the perturbation amplitude grows with time for $\alpha = -1$, where $\gamma = 1$, $q = -1$, for an initially flat surface. The perturbation takes a long time to start but once it starts the amplitude keeps growing steadily.

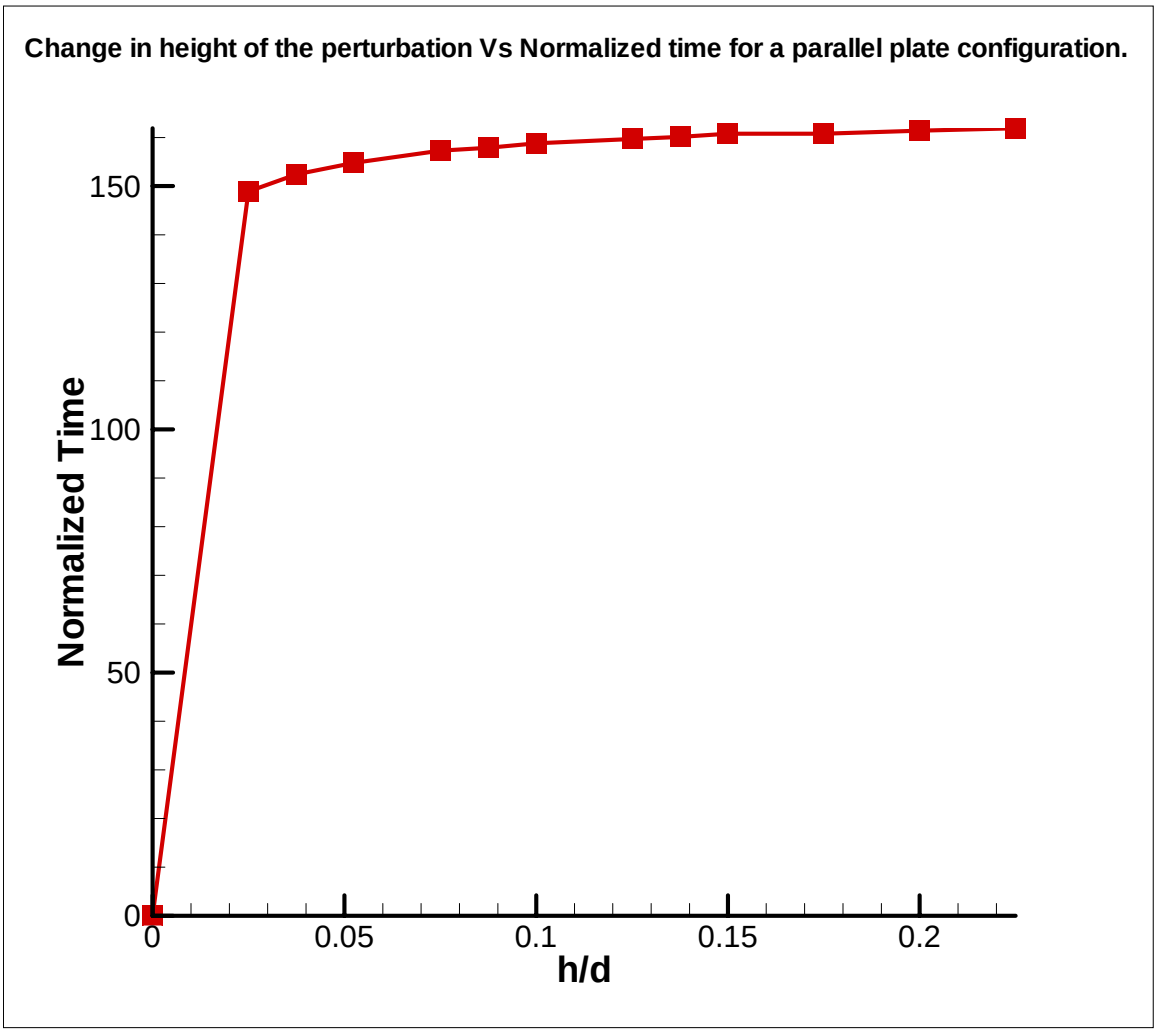

Figure 4.6: Change in amplitude of a perturbation vs. the normalized time for a parallel plate capacitor at α = -1.

The simulations discussed in this section show that a flat surface subjected to a uniform electric field is unstable. The growth rate of the perturbation is a strong function

of the applied electric field. For the flat surface, the perturbation takes a significant time to start but grows steadily afterwards.

Next, FEM analysis was carried out for a configuration similar to the experimental conditions, as shown in Fig. 4.2, where the width of the lower electrode is much longer than that of the upper electrode w. The gap between the electrodes is d. The overall length of the lower surface is kept much larger than the electrode width, w, in order to maintain zero flux points, A and B, in Fig. 4.1 far away from the fringe field. The analysis is carried out for a constant α, while the ratio w/d is varied in order to simulate the experiments in which the electrode width is varied. First the analysis is carried out for $\alpha = -1$, where $\gamma = 1$, $q = -1$, and $w/d = 10$, the results of which are shown in Fig. 4.7. The contours in Fig. 4.7 show the y-component of electric field. In the experiments the applied electric field is about *0.5-1 V/nm*, hence $\alpha = -1$ is a good approximation. The gold surface starts to evolve into two separate islands near the edges of the upper electrode. The islands are flanked by valleys on each side. The valley outside the electrode is the deeper of the two valleys, the depth of which is about half that of the peak. This surface evolution is quite similar to that in the Maxwell-Rogowski analysis in Chapter 2 (Section 2.5). One of the differences between the simulation and the analysis is the depth of the valley. Also the depth of the valley is shallower in simulation results as compared to the analytical analysis where the depth is same as the height of the hill.

There is some surface evolution in the interior uniform field region; however it is negligible compared to growth in the fringe field region. By the time, there is any appreciable growth in the uniform field region, the edge islands run into the upper

electrode. Note that the islands in the fringe field do not have an equilibrium height; they continue to grow until they contact the upper electrode.

Simulations were also carried out where the surface was given a small sinusoidal perturbation, $y = \eta Sin\left(\frac{2\pi x}{\lambda}\right)$, with amplitude, η, much smaller than d and $\lambda = \lambda_{cr}$ as given by Eq. 2.30 in Section 2.3.1. The objective of introducing this perturbation is to study the effects of surface roughness of the test surface before the experiment is conducted. As was reported in previous chapter the initial test surface has a roughness with peak to peak value of ~ 5 *nm*, which is quite small as compared to distance d = 250 *nm* between the electrodes. Fig. 4.8 shows the normalized time it takes for the perturbation to grow 0.6 times the distance d, under the fringe field, versus $Abs(\alpha)$, where $\gamma=1$ and $q=-1$. As can be seen in Fig. 4.8, the perturbation does not make any appreciable difference in the final result and the kinetics remains unaffected.

This set of simulations show the surface subjected to electric field using a finite electrode evolves into two separate islands forming under the electrode edges. The growth kinetics are dominated by the gradient/fringe field and the surface evolves much quickly as compared to the surface subjected to uniform field. This growth is unstable and the islands keep getting higher and higher until they run into the top electrode.

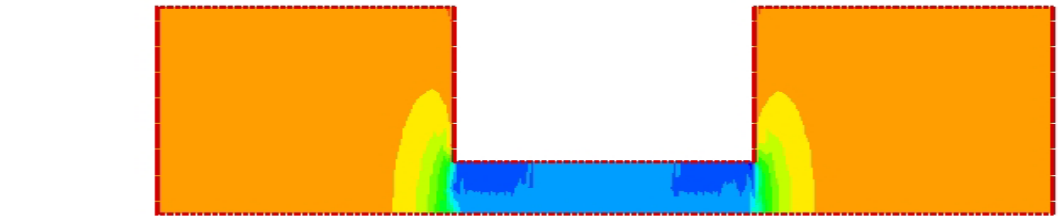

(a)

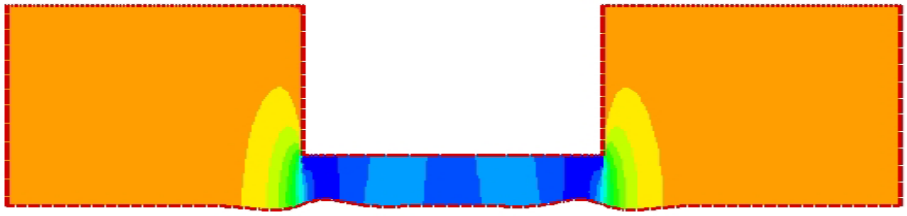

(b)

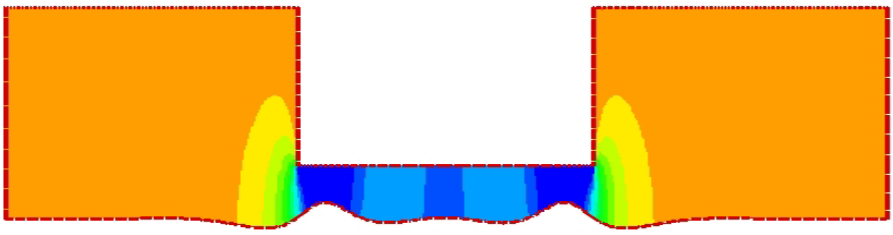

(c)

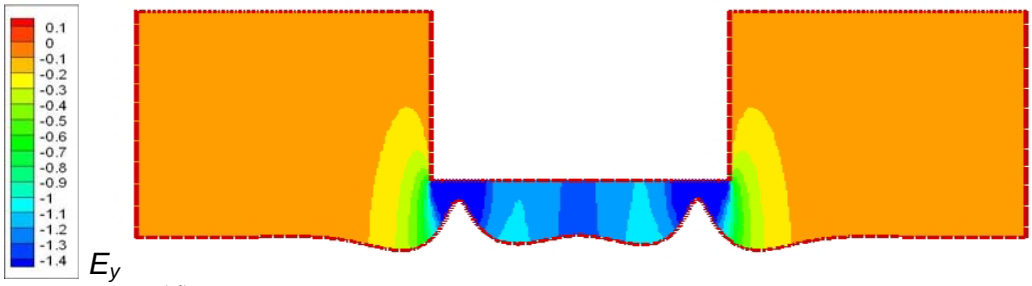

(d)

Figure 4.7: Results of FEM analysis for w/d=10, α = -1, where γ = 1, q = -1, showing evolution of surface into two separate islands under the electrode edge at (a) t/τ=0, (b) t/ τ =0.25, (c) t/ τ =0.6, (d) t/ τ = 0.75.

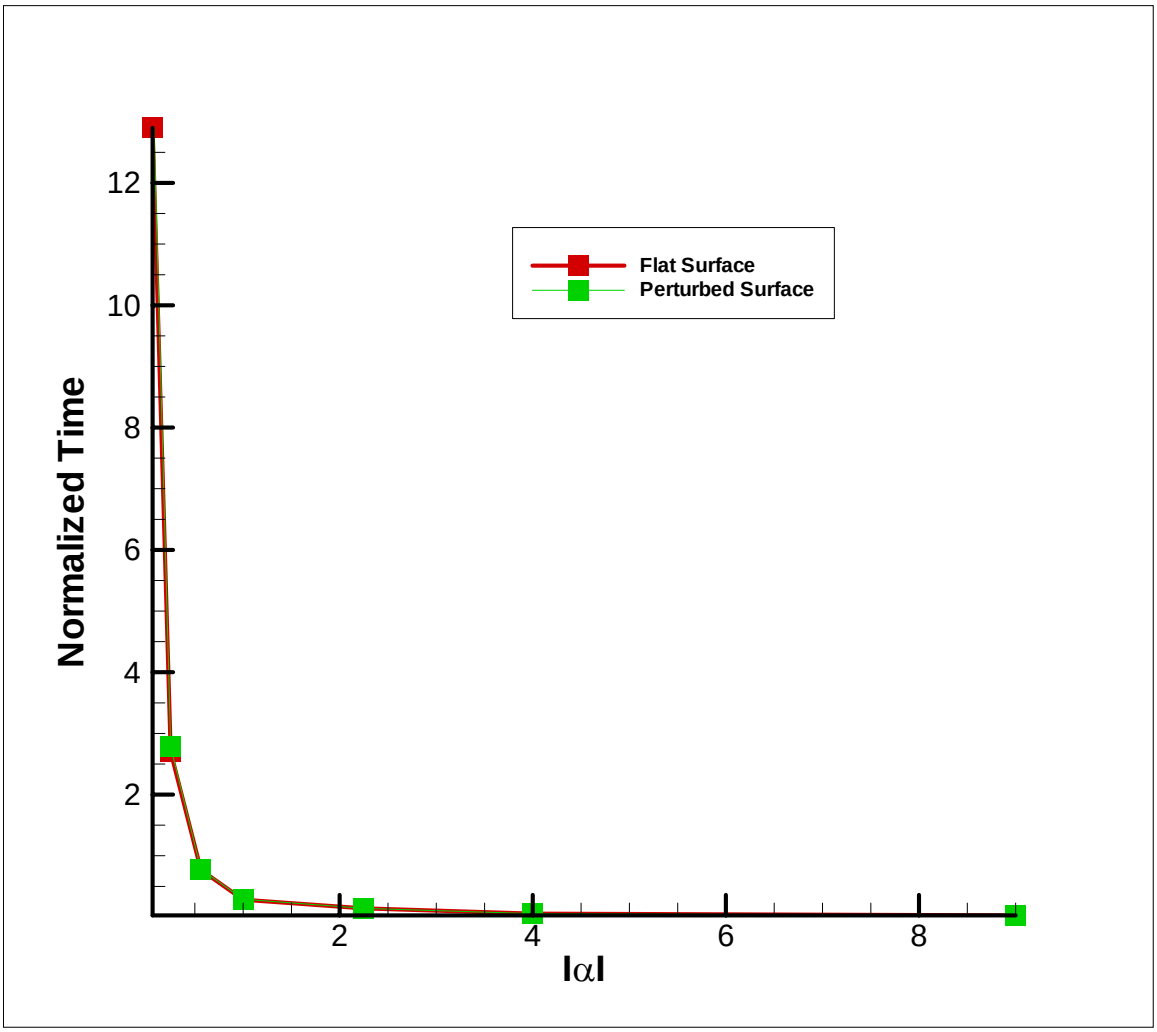

Figure 4.8: Normalized time (t/τ) versus Abs(α), where γ=1 and q=-1, for the perturbation amplitude to grow 60% of the initial distance d between the two electrodes for a perturbed and an initially flat surface.

Next, the FEM analysis was carried out for smaller values of *w/d*. As the ratio *w/d* is reduced at a constant *Abs(α)*, the two edge islands start to merge. A result of one such analysis is shown in Fig. 4.9. It can be seen that, for $\alpha = -1$, where $\gamma=1$ and $q=-1$, at $w/d =$ 4.4, the two edge islands start to interact and merge near the center of the electrode.

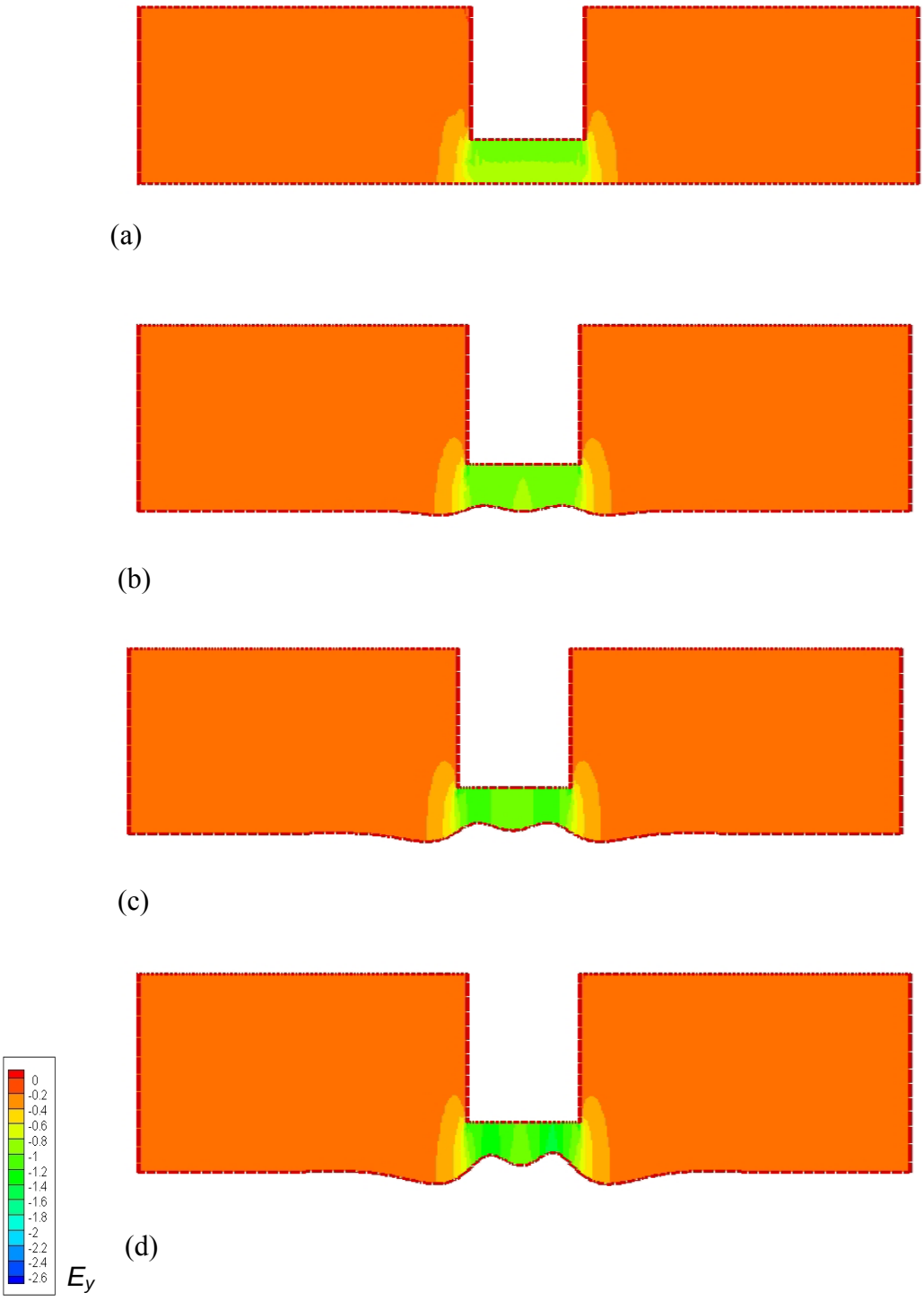

Figure 4.9: Results of FEM analysis for w/d=4.4, α = -1, where γ=1 and q=-1, showing evolution of surface into two separate islands trying to merge at the center of the electrode edge at (a) t/τ=0, (b) t/ τ =0.25, (c) t/ τ =0.65, (d) t/ τ = 0.95.

As the ratio *w/d* is further reduced, the two edge islands transition into a single island forming under the electrode at *w/d* = 3.5 for α = -1, where $\gamma = 1$ and $q = -1$, as shown in Fig. 4.11. There is a critical value of *w/d* for any given α where the double island transitions into a single island. This critical transition width is plotted in Fig. 4.10. This transition from double island to single island happens over a very narrow range of *w/d* values. This happens at the point where the bases of the two edge islands start to touch each other. The base width if the islands is determined by the magnitude of α. As the magnitude of the applied electric field is increased, the islands become sharper and their base width decreases. Hence the double island changes to single island at decreasing *w/d* values and for increasing *Abs(α)* values as seen in Fig. 4.11. The islands grow much quicker in the vertical direction for a higher applied electric field as compared to the growth of their base. Hence these islands run into the upper electrode before their bases can interact and form a single island. In the case of lower electric field, the vertical growth process slows down as can be seen in Fig. 4.8. This gives the bases of two islands to grow farther out, interact and merge to form a single island.

The applied electric field in the experiments is about 0.5 *V/nm* and the distance *d* between the electrodes is 250 *nm*. According to Fig. 4.10, the transition from double to single island should happen at *w/d* = 7, hence at $w = 7d = 1750$ *nm*. In the experiments this transition is seen around 2.5-3.0 μm. Hence the simulation is quite close in predicting the transition width.

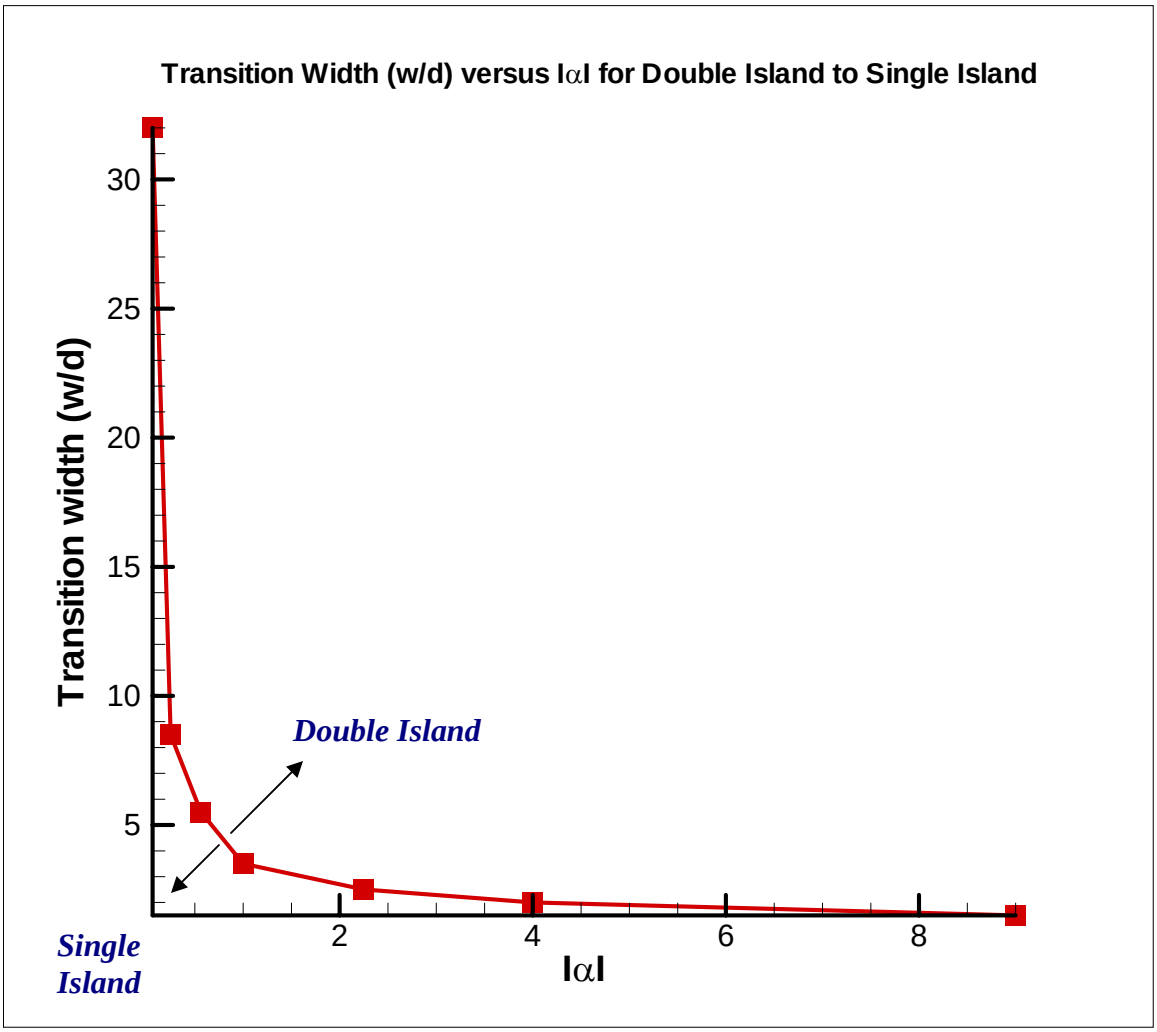

Figure 4.10: w/d ratio versus Abs(α), where γ=1 and q=-1, for the double island to transition into a single island.

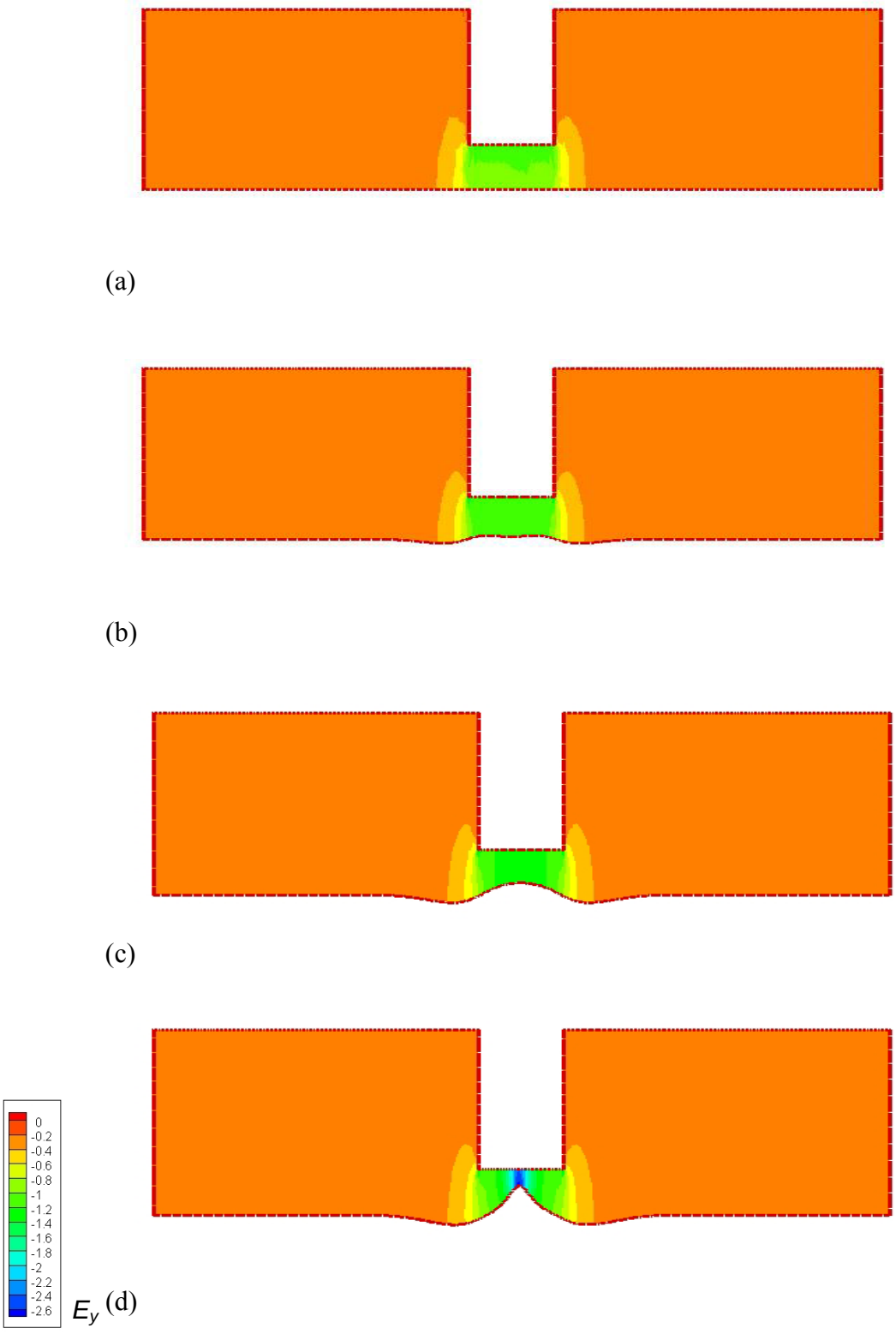

Figure 4.11: Results of FEM analysis for w/d=3.5, α = -1, where γ=1 and q=-1, showing evolution of surface intone single island under the electrode edge at (a) t/τ=0, (b) t/ τ =0.25, (c) t/ τ =0.55, (d) t/ τ = 0.69.

4.5 Growth Kinetics

In the numerical procedure the time is normalized by a parameter τ given by Eq. 4.9. The real time can be calculated by multiplying τ with the normalized time t_o. In the code the diffusivity D_s and the temperature T, in Kelvin, during the experiment is determined by a parameter β given by Eq. 4.15. For all the results presented in this chapter β is set to a value of 1.

$$\beta = \frac{\Omega D_o C_s \exp(-Q_s/kT)}{kT} = \frac{\Omega D_s C_s}{kT} \tag{4.15}$$

where Q_s is the activation energy for surface diffusion.

The normalizing parameter then becomes

$$\tau = \frac{d^4}{\beta \Omega \gamma} \tag{4.16}$$

For surface energy γ = 1 J/m^2, temperature T = 550 K, the distance between the two electrodes d = 250 nm, β = 1, atomic volume Ω = 1.3 x 10^{-29} m^3, τ = 300 s, which is a little low. The numerical time is about one order of magnitude lower than the observed time. The difference can be attributed to lower surface energy in the experiments than 1 J/m^2 considered for the simulation.

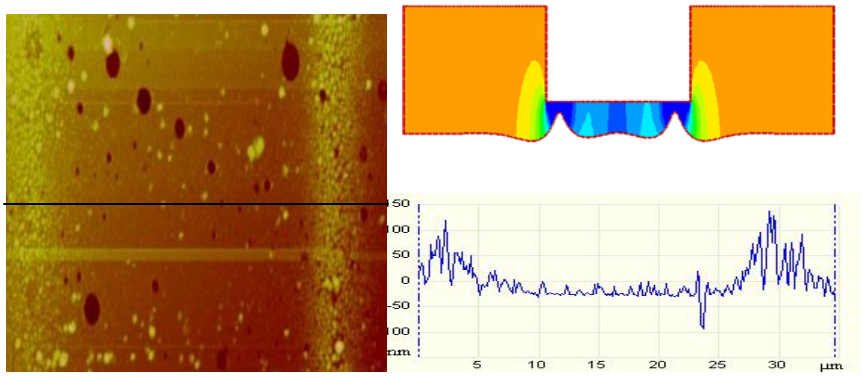

(a)

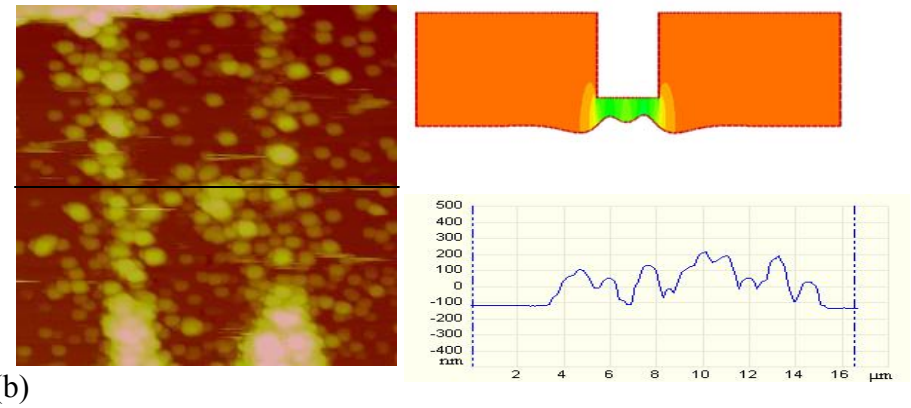

(b)

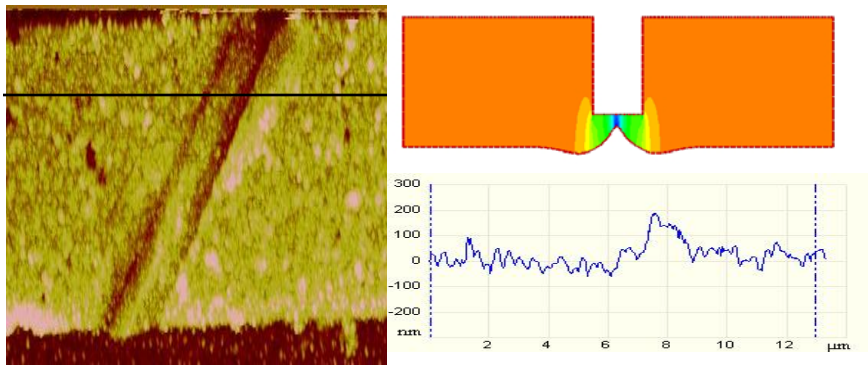

(c)

Figure 4.12: Comparison between the experimental results with line scans along the dark line and FEM results, (a) Large electrode size (~25 µm), (b) Medium electrode size (8 µm), (c) Small electrode size (1.5 µm).

4.6 Conclusions

The FEM analysis qualitatively captures the transition in the experimental results, from two bands of islands for a wide electrode to a single ridge for a thin electrode. A comparison between experimental results and results from numerical modeling can be seen in Fig. 4.12. The numerical modeling shows the transition from double edge islands to single ridge under the electrode as observed in experiments. The simulation shows double island growth at $w/d = 8$ for $\alpha = -0.25$, where $\gamma=1$ and $q=-1$,. For $d = 250$ *nm*, that predicts a double island for $w = 2$ μm for an applied field of 5×10^8 *V/m*. But in experiments the double island is observed for $w > 10$ μm. But this is less than one order of magnitude discrepancy; otherwise the simulation results are quite satisfactory. The main results of the numerical modeling can be summarized as below.

- The analysis shows the dominance of island growth near the edges compared to the instability driven growth near the center of the electrode. The analysis also shows that the growth rate is much faster in the gradient field region as compared to the uniform field region in the interior.
- The growth time for the perturbation is proportional to $1/E^4$, where E is the applied electric field. This is consistent with the trend for growth time versus applied electric field one gets from analytical solution.
- The analysis shows that the growth kinetics is much faster in the gradient field region as compared to the uniform field region in the interior which is again consistent with both the analytical model and the experimental results.

- A single ridge can be obtained for a given electrode width if a low enough electric field is used but the time needed to grow this island becomes very large and not practical.
- As the electrode width is reduced, for a given applied electric field, there is a transition from two edge islands, which begin to merge, and they form a single island as the electrode width is further reduced.
- The simulation gives a reasonabe estimation of the transition width of the electrode from double to single island for a given electric field.

Chapter 5

Concluding Remarks

5.1 Summary

The work presented here investigates the phenomenon of electric field induced surface diffusion on conducting solids. The basic motivation is provided by the possibility of using the phenomenon to develop a fabrication method for patterned islands of any size distribution. The electric field provides driving force for material to diffuse over the surface and form micro/nano scale features.

Driving force on a conducting surface due to electric field is demonstrated through an energetic argument, by showing that the potential energy of an electrode – conductor surface system can be minimized by island-like surface perturbations under the electrode. Further, it is shown that, electric field can induce surface evolution in two ways. In the presence of a uniform field, perturbations above a critical wavelength get destabilized, similar to strain induced instability. Alternatively, a non-uniform electric field provides the surface chemical potential gradient for mass diffusion and surface evolution. In most practical experimental configurations, presence of edges and the corresponding fringe fields are inevitable, which provide a natural location for surface evolution. An estimate of the growth time constants reveals that the growth rates in the fringe fields are usually significantly higher than those for the instabilities in the uniform region.

Motivated by the results of the analysis, which suggested that islands of sub-micron height can be grown with sufficiently high electric fields, an experimental setup was developed to realize the analytical predictions. The experiments showed that:

- Bands of islands grow near the edges under the influence of the gradient/fringe field.
- As the electrode width is decreased, the bands begin to merge. Eventually, for a width of 1.3 μm, multiple islands were replaced by a single ridge, demonstrating the feasibility of growing isolated islands of sufficiently small length scale.
- In all experiments considered, instability within a uniform field was not observed; only surface evolution due to gradient field was observed. It was estimated from growth kinetics that, for the experimental geometry under consideration, the rate of growth due to the fringe field is much greater than that due to the uniform field, which is consistent with the observations.
- Thermal roughening due to grain boundary grooving competes with surface evolution due to electric field. In future studies, single crystal gold surfaces are recommended.
- Numerical simulations based on finite element method were carried out to gain further insight into kinetics. The simulations capture the observation that the two edge islands merge into one when the electrode width is reduced below a critical value.
- Although this work demonstrates the phenomenon of electric field induced surface diffusion, more understanding and systematic investigation is necessary before it can be used to develop a fabrication method based on it.

In summary existence of electrical configuration force on conducting surface was demonstrated. This force can drive surface diffusion at physically useful length scales.

This process of surface diffusion can be guided by applying the electrical field at selective locations.

5.2 Future Work

The work presented here is essentially a proof of concept work, demonstrating that micro/nano-scale features can be created over conducting surfaces. Also the formation of these features can be spatially controlled by applying external electric fields. This technique can be further refined using more improved experimental techniques.

In the foregoing discussion in previous chapters, any residual stress in the sample layer has been ignored while considering the competition between the electric field energy and the surface energy. Usually, stress of the order of 1 GPa or more is necessary for elastic energy to play a significant role in surface evolution. Thus, ignoring elastic stresses is justified in sufficiently thick metals films with low yield stress such as gold (~ 100 MPa). However, thin confined metal films can sustain stresses of the order of 1 GPa. Moreover, stresses of the order of 1 GPa or more are common in semiconductor thin films and in films of so-called low mobility materials such as diamond. In such cases, it will be necessary to consider the combined influence of the elastic energy and the electrostatic energy on surface evolution. For a sinusoidally perturbed surface considered in section 2.3, it can be shown that, in the combined presence of a sample stress σ and an electric field E, the growth rate of the amplitude (η) of a perturbation of wavelength λ can be written as

$$\dot{\eta} = \left(\frac{16\pi^3 \left(1-\nu^2\right)\sigma^2}{E\lambda^3} + \frac{4\pi^2 \varepsilon_o E^2}{d\lambda^2} - \frac{16\pi^4 \gamma}{\lambda^4} \right) \eta \qquad (5.1)$$

where the first two terms in the parenthesis on RHS are destabilizing terms due to stress and electric field respectively, whereas the third term is the stabilizing term due to surface energy. From Eq. (5.1) it is clear that the electric field and the elastic field "work together" to destabilize the surface. Thus, in stressed films, it would be easier to achieve "guided assembly" of isolated islands through focused electric field since the existing stress can provide the primary driving force and the electric field needs to provide only an additional guiding force to initiate an island at a targeted site. In case of a uniformly strained film, driving force for instability is equally present everywhere on the film. As a result, the final locations of the islands are determined by random initiation sites determined by surface perturbations. Using focused electric fields of sufficiently high magnitude, it should be possible to control the island nucleation sites. Thus, the possibility of combining elastic and electric driving forces to achieve controlled pattern growth appears to be a promising area of future research.

Thermal roughening is a problem associated with the current set of experiments discussed in this thesis. Future experiments should be carried out with single crystal samples, thus minimizing the effect of thermal roughening. This will enable the experiments to be carried out at significantly higher temperatures than those in the present study and will quicken the kinetics of micro/nano-structure growth. Also, it would be desirable to carry out such experiments in ultra-high vacuum (UHV) conditions to minimize oxidation.

Appendix A

Driving force in 3-D case

The same analysis can be carried out for a 3-D case. An electrode with width *w* and depth *h* is considered for this case. The initial perturbation on the surface is

$$z = \eta \, Cos \left(\frac{\pi x}{w} \right) Cos \left(\frac{\pi y}{h} \right) \tag{A.1}$$

The change in capacitance of the system due to the introduction of this perturbation can be calculated as

$$C_2 - C_1 = \varepsilon_o \int_{\frac{-w}{2}}^{\frac{w}{2}} \int_{\frac{-h}{2}}^{\frac{h}{2}} \left[\frac{dxdy}{d - z} - \frac{dxdy}{d} \right] \tag{A.2}$$

Now in the case when the perturbation amplitude η is much smaller than the distance *d* between the electrode and the surface, the change in electric potential of the system can be found as

$$\Delta U_E = \frac{2 \varepsilon_o V^2 \eta wh}{\pi^2 d^2} \tag{A.3}$$

Now, the change in surface energy due to the perturbation can be calculated as

$$\Delta U_S = \frac{\gamma \pi^2 \eta^2 \left(h^2 + w^2 \right)}{8 hw} \tag{A.4}$$

The net change in the potential energy of the system is

$$\Delta U = \frac{\gamma \pi^2 \eta^2 \left(h^2 + w^2 \right)}{8 hw} - \frac{2 \varepsilon_o V^2 \eta wh}{\pi^2 d^2} \tag{A.5}$$

Once again the equilibrium perturbation amplitude can be calculated by

$$\frac{d\,\Delta\,U}{d\,\eta} = 0 \tag{A.6}$$

Hence

$$\eta_o = \frac{8\,\varepsilon_o V^2 w^2 h^2}{\pi^4 d^2 \gamma \left(h^2 + w^2\right)} \tag{A.7}$$

Now for a square electrode where $h = w$

$$\eta_o = \frac{4\,\varepsilon_o V^2 w^2}{\pi^4 d^2 \gamma} \tag{A.8}$$

Appendix B

Stability for a 3-D case

In the previous section the stability of a 1-D surface was analyzed. In this section a similar analysis for a 2-D surface is carried out. A 2-D surface in a parallel plate configuration with an initial perturbation

$$z = \eta \, Sin \left(\frac{2 \pi x}{\lambda_1} \right) Sin \left(\frac{2 \pi y}{\lambda_2} \right) \tag{B.1}$$

is considered. Here again, perturbation amplitude η is much smaller as compared to the distance between the two plates. The perturbation has a wavelength λ_1 in the *x*-direction and a wavelength, λ_2 in the *y*-direction. The initial capacitance before the perturbation is given by

$$C_1 = \frac{\varepsilon_o \lambda_1 \lambda_2}{d} \tag{B.2}$$

The final capacitance after the perturbation can be calculated as

$$C_2 = \varepsilon_o \int_0^{\lambda_1} \int_0^{\lambda_2} \frac{dxdy}{d - z} \approx \frac{\varepsilon_o}{4d} \left(4 + \frac{\eta^2}{d^2} \right) \lambda_1 \lambda_2 \tag{B.3}$$

Hence the change in electric potential energy of the system is given as

$$\Delta U_E = - \frac{\varepsilon_o V^2 \eta^2 \lambda_1 \lambda_2}{8 d^3} \tag{B.4}$$

The change in surface energy of the system due to the introduction of the perturbation can be calculated as

$$\Delta U_S = \gamma \left[\int_0^{\lambda_1} \int_0^{\lambda_2} \left(\sqrt{1 + z_{,x}^2 + z_{,y}^2} - 1 \right) dxdy \right] \tag{B.5}$$

which can be simplified to get

$$\Delta U_S \approx \frac{\gamma \eta^2 \pi^2 \left(\lambda_1^2 + \lambda_2^2 \right)}{\lambda_1 \lambda_2} \tag{B.6}$$

Hence the total change in energy is

$$\Delta U = \frac{\gamma \eta^2 \pi^2 \left(\lambda_1^2 + \lambda_2^2 \right)}{\lambda_1 \lambda_2} - \frac{\varepsilon_o V^2 \eta^2 \lambda_1 \lambda_2}{8 d^3} \tag{B.7}$$

If the perturbation wavelength is same in both directions, ie. $\lambda_1 = \lambda_2$ then the change in energy is given by

$$\Delta U = \eta^2 \pi^2 \gamma - \frac{\varepsilon_o V^2 \eta^2 \lambda^2}{8 d^3} \tag{B.8}$$

Similar to the previous section a critical wavelength can be calculated by setting $\Delta U = 0$.

$$\lambda_{cr}^2 = \frac{4 d^3 \pi^2 \gamma}{\varepsilon_o V^2} \tag{B.9}$$

which is same as the 1-D case.

Appendix C

Sample Fabrication

Sample fabrication begins with a clean, square glass substrate of 12.5mm side length and 1mm thickness. A 1.2 μm layer of positive photoresist (Shipley 1813, Microchem, MA) is coated on the glass substrate, by spinning at 5000 *rpm* for 30 *s*. Photolithography is carried out using an appropriate mask on a Karl Suss MJB3 mask aligner. The sample is exposed for approximately 30 seconds. This sample is then developed by completely dipping it in a 1:1 solution of DI water and MF-312 (Tetramethylammonium Hydroxide) for about 45 *s*. The sample is then cleaned using DI water and dried with a dry nitrogen gun. This sample is cleaned in a Reactive Ion Etcher using oxygen plasma for about 2 *minutes*. This plasma cleaning is carried out so that no residual resist is left on the substrate where the resist was exposed and etched away after developing. A thin layer of titanium, about 10 *nm* thick, is then deposited on the sample using an electron-beam evaporator, which promotes adhesion of gold to glass substrate. Next, a thin film of gold, about 200-225 *nm* in thickness is deposited on top of this titanium layer. The sample is then immersed in acetone for about 24 *hours* for lift off, following which, only the thin gold lines are left where the photo resist was exposed during the photolithography step and the rest gets removed.

In order to deposit the alumina film, the same photoresist is spin coated on the glass plate with gold lines on it. By photolithography, the photoresist is removed everywhere except along the gold lines, as illustrated in Fig. 3.2 (d) and (e). This sample is plasma cleaned and a layer of Aluminum Oxide, about 400-425 *nm* is deposited by electron-beam evaporation. Once again the sample is left in acetone for 24 *hours* to lift away the resist.

The final sample is a series of gold lines running parallel to each other, flanked by alumina films, which are about 200 *nm* taller.

References:

Avouris ,P.(1995). Manipulation of matter at the atomic and molecular levels. *Accounts of Chemical Research* (28) 95-102.

Boke, H., Cizer, O., Ipekoglu, B., Ugurlu, E., Serifaki, K. Toprak, G. (2008). Characteristics of lime produced from limestone containing diatoms, *Construction and Building Materials* (22) 866-874.

Chien, N.Y., Gao, H., Herrmann, G. and Barnett, D.M. (1996). Diffusive surface instabilities induced by electromechanical loading. *Proceedings: Mathematical, Physical and Engineering Sciences* (452) 527-541.

Chiu, C.H-.,Poh,C.T. and Huang,Z. (2006a). Morphological stability of the Stranski-Krastanow systems under an electric field. *Applied Physics Letters* (88) 241906.

Chiu,C.H-.,Huang,Z. and C. T. Poh (2006b). Formation of nanoislands by the electromolding self-organization process. *Physical Review* (B 73) 193409.

Chou,S.Y. and Zhuang,L. (1999a). Lithographically induced self-assembly of periodic polymer micropillar arrays. *Journal of Vacuum Science and Technology B: Microelectronics and Nanometer Structures* (17) 3197-3202.

Chou,S.Y.,Zhuang,L. and Guo,L.J. (1999b). Lithographically induced self-construction of polymer microstructures for resistless patterning. *Applied Physics Letters* (75) 1004-1006.

Chuang, T. and Rice, J.R. (1973). The shape of intergranular crep cracks growing by surface diffusion. *Acta Mettalurgica (21)* 1625-1628.

Cobine,J.D. Gaseous Conductors. *McGraw-Hill Book Company, New York*, 1941.

Du,D. and Srolovitz,D. (2004) Electrostatic field-induced surface instability. *Applied Physics Letters* (85) 4917-4919.

Dulot,F., Eugene,J., Kierren,B., Malterre,D. (2000). STM-TIP induced surface diffusion of copper on copper (100). *Applied Surface Science* (162-163) 86-93.

Freund,L.B. (1995). Evolution of waviness on the surface of a strained elastic solid due to stress driven diffusion. *International Journal of Solids and Structures* (32) 911-923.

Gill, V., Guduru, P. and Sheldon, B. (2008). Electric field induced surface diffusion and micro/nano-scale island growth. *International Journal of Solids and Structures* (45) 943-958.

Horn, K.M., Chason, E., Tsao, J.Y., Floro, J.A. and Picraux, S.T. (1994). Oxygen roughening of Ge (001) surfaces. *Surface Science* (320) 174-184.

Kim,D. and Lu,W. (2006a). Interface instability and nanostructure patterning. *Computational Materials Science* 38 (2) 418-425.

Kim,D. and Lu,W. (2006b). Three-dimensional model of electrostatically induced pattern formation in thin polymer films. *Physical Review* B 73 (3): Art. No. 035206.

Leach,K.A., Gupta,S., Dickey,M.D., Willson,C.G. and Russell,T.P. (2005). Electric field and dewetting induced hierarchical structure formation in polymer/polymer/air trilayers. *Chaos* (15) 047506.

Lei, X., Wu, L., Deshpande, P., Yu, Z., Wu, W., Ge, H. and Chou, S.Y. (2003). 100nm gratings produced by lithographically induced surface construction. *Nanotechnology* (14), 786-790.

Li,J., Berndt,R., Schneider,W-D. (1996). Tip-assisted diffusion of Ag(110) in scanning tunneling microscopy. *Physical Review Letters* (76) 1888-1891.

Lu, W. and Kim,D. (2006). Thin film structures induced by electrostatic field and substrate kinetic constraint. *Applied Physics Letters*, 88 (15): Art. No. 153116.

Maxwell,J.C. A Treatise on Electricity and Magnetism, *Dover publications*, 1979.

Medeiros-Ribeiro, G., Bratkovski, A. M., Kamins, T. I., Ohlberg, D. A. A. and Williams, R. S. (1998). Shape transition of germanium nanocrystals on a silicon(001) surface from pyramids to domes. *Science* 279(5349), 353–355.

Murphy,S., Osing,J. and Shvets,I.V. (2003) Irreversible nanoscale morphology transformation of an Fe film on Mo(1 1 0) induced by a magnetic STM tip. *Surface Science* (547) 139-148.

Philibert,J. Atom Movements. Diffuion and Mass Transport in Solids. *Les Editions de Physique,* 1991.

Rogowski,W. *Arch. f. Elekt.*(12) 1, 1923.

Rubinstein, A.A.(1983). Diffusive relaxation of stress concentrations at grain boundary cavities in elevated temperature creep. *International Journal of Engineering Science* (21) 593-616.

Schaeffer,E., Thurn-Albrecht,T., Russell,T.P. and Steiner,U. (2000). Electrically induced structure formation and pattern transfer. *Nature* (403) 874-877.

Srolovitz,D.J. (1989). On the stability of surfaces of stressed solids. *Acta Metallurgica* (37) 621-625.

Suo,Z. and Liang,J. (2001). Theory of lithographically-induced self-assembly. *Applied Physics Letters* (78) 3971-3973.

Xia, L., Bower, A., Suo, Z., and Shih, C. (1997). A finite element analysis of the motion and evolution of voidsdue to strain and electromigration induced surface diffusion. *Journal of the Mechanics and Physics of Solids* (45), 1473-1493.

Xiang,H., Lin,Y. and Russell,T.P. (2004). Electrically Induced Patterning in Block Copolymer Films. *Macromolecules* (37) 5358-5363.

Yang,F. and Song,W. (2005). Morphological instability of elastic thin films–effect of electromechanical interaction. *Applied Physics Letters* (87) 111912-1.